Stability analysis of velocity feedback for the plasma vertical instability in fusion tokamaks

Stability analysis of velocity feedback for the plasma vertical instability in fusion tokamaks

M.J. (Maarten) Beelen

CST 2010.031

Report of Master traineeship

Supervisory committee:

Dr. M.L. Walker[1]
Ir. G. Witvoet[2]
Dr. E. Schuster[3]
Prof. dr. ir. M. Steinbuch[2]

[1] General Atomics, San Diego
DIII-D Plasma Control and Operations Group

[2] Eindhoven University of Technology
Department of Mechanical Engineering
Control Systems Technology Group

[3] Lehigh University
Department of Mechanical Engineering and Mechanics
Complex Physical System Control Laboratory

Eindhoven, June 2010

A personal message

from the author

Although only in the first part of my master Mechanical Engineering, I already had the opportunity to work on two motivational projects, involving a nuclear fusion reactor and a bioreactor. What motivates me is what they have in common. Albeit a great scientific challenge, nuclear fusion has the potential to become a huge contribution to our sustainable energy supply. Some major advantages are the 'fuel' that is abundantly present on earth, the minimal nuclear waste, no emission of greenhouse gasses and its nonexplosive character. A bioreactor for cultivating tissue engineered aortic heart valves could help enabling medical treatments for many patients and significantly improve their well being compared to conventional heart valve replacements.

These goals are grand, the contributions seemingly small.

As every person part of society, a mechanical engineer can purposely choose what goals to devote his efforts to, especially judging from technology's key role at present. Although many of world's problems are much debated and complexified, often endeavors can simply be brought down to being either destructive or constructive. Shortsighted or broad visioned. Weapon intelligence or refugee shelters. Oil depletion or alternative energy sources. Smart bullets or medical innovations.

Although some contributions might seem small, depreciating one's influence takes away one's responsibility. Not a single individual can achieve these goals. With enough of us committed, we might just accomplish them.

Maarten J. Beelen
m.j.beelen@student.tue.nl
June 30, 2010

Stability analysis of velocity feedback for the plasma vertical instability in fusion tokamaks

M.J. Beelen, M.L. Walker, G. Witvoet, E. Schuster, M. Steinbuch

Abstract— **The source of the vertical instability in tokamaks is relatively well understood, and stabilizing controllers have been successfully implemented in numerous tokamaks. Usually these controllers are designed based on a plasma model that assumes the plasma has zero mass. In reality the plasma mass is small but positive, so that some of the controller designs yield an unstable closed loop.**

In this work we expand on [1], further investigating the discrepancy between the massless plasma model and the plasma with mass model. It turns out that conclusions about closed loop behavior depend on the controller's asymptotic behavior at infinite frequency. Simulations on models of KSTAR and ITER are performed with varying presence of passive stabilizing structures, including the possibility of superconductive control coils. It is shown that erroneous conclusions regarding asymptotic stabilization only result from non proper controllers. The results confirm that neither pure velocity feedback nor a proper or strictly proper form of velocity feedback can asymptotically stabilize the vertical instability.

I. Introduction

NUCLEAR fusion is the source of virtually all of the energy of the universe. The sun and stars shine due to fusion, supporting all life on earth. Our fossil fuels, including coal, oil and gas, are stored sunshine, that is, stored fusion energy.

Achieving controlled fusion on earth is one of the great challenges of science, but it has a large potential as a source of sustainable energy. The fuels needed for fusion, deuterium and tritium, can be obtained from water and from lithium respectively, which are abundantly present on earth. Without the emission of greenhouse gasses, the low amount of nuclear waste in terms of volume and half-life, and its non-explosive character due to the absence of chain reactions (in contrast to fission), a fusion-power reactor would offer significant advantages over existing energy sources.

To initiate and sustain fusion reactions, a gas comprised of ionized hydrogen isotopes, called a plasma, has to be heated and confined. Three known ways to confine the plasma are gravitational confinement (like the sun), inertial confinement (controlled implosions) and magnetic confinement. Magnetic confinement uses magnetic fields exerting forces on the moving ionized particles.

The most promising of several magnetic confinement devices are tokamaks, devices constructed in the shape of a torus. The plasma in a tokamak is confined by means of an external helical magnetic field generated by a set of coils distributed around the vacuum vessel and the plasma currents. The two main components of this field are the toroidal field B_T, generated by toroidal field (TF) coils, and the poloidal field B_P, generated by the plasma current, which is induced by a transformer action. Moreover, a strong vertical field B_Z is needed to counteract the plasma hoop force. This force is directed radially outward, and is caused by plasma pressure trying to expand the plasma ring, and the self exerted Lorentz force. The vertical field is generated by a set of poloidal field (PF) coils. These coils have the additional purpose of changing the shape and position of the plasma.

A. Plasma Vertical Instability

Although the first tokamaks allowed only for plasmas having a circular cross-section, modern advanced machines usually operate with plasmas which have a vertically elongated (D-shaped) cross-section; this is important to assure better fusion performance and it allows better filling of the vacuum chamber. To achieve a vertically elongated plasma, a radial component has to be added to the vertical magnetic field distribution (see Fig. 1), using the PF (shaping) coils. This component is directed inward above the midplane, and directed outward below the midplane which causes an upward force acting on the top of the plasma and a downward force acting on the bottom of the plasma. But the equilibrium among these forces that elongate the plasma is unstable. When a disturbance shifts the plasma up slightly, more current moves above the midplane and the net force is directed upward. This imbalance causes the plasma to move up, thereby further increasing the upward force. This behavior causes the appearance of a vertical unstable mode. When no corrective action would be taken, the hot plasma column would move vertically in a fraction of a second until it reaches the protecting tiles and it would terminate rapidly.

The growth time of the vertical instability would be on the Alfvén time scale (a few microseconds or less), were it not for the stabilizing influence of induced currents in passive conducting structures. These currents generate forces that oppose the plasma movement. The resistance of the passive structures determines the time needed for the induced currents to decay away. This time scale, called the resistive wall time, governs the growth time of the vertical instability,

M. J. Beelen (email: m.j.beelen@student.tue.nl), G. Witvoet and M. Steinbuch are with the Eindhoven University of Technology, Dept. of Mechanical Engineering, Control Systems Technology group, P.O.Box 513, 5600 MB Eindhoven, the Netherlands.

M. L. Walker is with General Atomics, San Diego, CA 92121 USA

E. Schuster is with the Lehigh University, Bethlehem, PA 18015 USA

and is in the order of a few milliseconds. Theoretically, the instability can be (marginally) stabilized when the plasma is surrounded with a structure that is superconductive. But standard conductive walls with positive electrical resistance can only reduce the growth time of the unstable mode. As a consequence, to stabilize the plasma, an active feedback system is required that produces a radial magnetic field across the plasma in response to some measure of the plasma vertical position.

B. Objectives

In [1] the authors illustrate how analyses using a plasma model that assumes the plasma has zero mass can reach erroneous conclusions. This model can lead to feedback gains of the wrong sign, making the growth rate of the closed loop system even larger than the original open loop growth rate. In [2] the characteristic polynomials of a massless plasma model and a plasma with mass model were used to derive necessary and sufficient multivariable conditions for stabilization of a plasma model that incorporates the plasma mass, by feedback based on a massless plasma analysis. These results are based on PD-feedback as a prototype controller. The paper [1] also addresses the issue of pure velocity feedback and shows that this form of feedback cannot asymptotically stabilize the vertical instability.

When external control circuits and power supplies are accounted for, controllers that are implemented generally are strictly proper. Therefore, the pure PD form does not provide a representative simplification of practical controllers [2]. This work verifies the conclusions of [2] about closed loop behavior are dependent on the controller's asymptote at high frequencies. From this the question arises what will happen with a derivative controller that is proper, or strictly proper. In this work, stabilization by velocity feedback is further investigated. The results of [2] are examined in the context of a (strictly) proper derivative controller. Simulations are performed on different KSTAR and ITER plasma-coil-vessel configurations to investigate closed loop stabilization of different controllers, including the possibility of super conductive control coils. Both the massless plasma model and the plasma with mass model are considered, to investigate the erroneous conclusions of the massless plasma analysis described in [2], and a link is made with the conditions for stabilization of [1]. Throughout the analyses, excursions to the frequency domain are made whenever convenient.

In section II, two closely related models of the tokamak-and-plasma system are established. One model assumes massless plasma, the other model includes the mass in the analysis. The difference between the two models is investigated in section III, using a theoretical approach of a single coil model (section III-B) with a general form of controllers, a two circuit model (section III-C) and a n-conductor model (section III-D). The findings are verified by simulations in section V. In section V also simulation results from more complex multivariable tokamak plasma models are presented. From the acquired insight hypotheses are distilled that lead to some future work propositions.

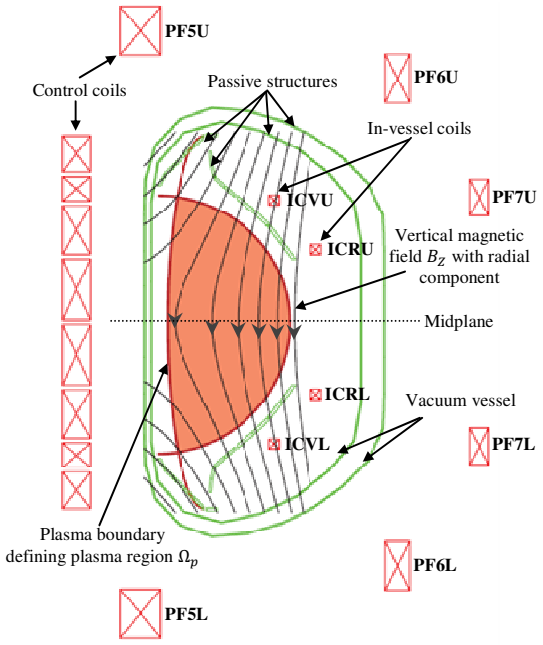

Fig. 1. Cross-section of the KSTAR tokamak in Daejon, South-Korea, containing a vertically elongated plasma, the vertical magnetic field distribution and Poloidal Field (PF) coils system.

II. MODELING

The plasma is modeled as a constant spatial distribution of plasma current, free to move vertically and radially, and is assumed to be axisymmetric. The various current-carrying elements (conductors) of a tokamak can interact mechanically with the plasma through the magnetic fields produced by these currents. The force equations describing these interactions are combined with linearized coil circuit equations that describe the electrical interactions, to form the dynamical model plant of the plasma-vessel-coils system used for control development [5]

$$M\dot{I} + R\delta I + \Psi_z \dot{z}_C + \Psi_r \dot{r}_C = U\delta V \ , \qquad (1)$$

where the state vector I contains the currents in the toroidal conductors, while $\delta I = I - I_{eq}$ represents a perturbation from the nominal plasma equilibrium I_{eq}. The n conductors include the n_c PF active control coils, consisting of shaping coils and central solenoid (CS) coils, and the n_v passive structures such as vessel elements, which are indicated in Fig. 1. The perturbation of the toroidal voltages on the conductors is represented by $\delta V = V - V_{eq}$. To make a distinction between the passive and active circuits the mapping matrix $U^T = [\boldsymbol{I}_{n_c} \quad \boldsymbol{O}_{n_c x\, n_v}]$ is used [3]. The identity matrix $\boldsymbol{I}_{n_c}$ corresponds to the voltages that are

applied to the active control coils provided by external voltage sources. The zero matrix $\boldsymbol{O}_{n_v x\, n_c}$ corresponds to the passive circuits (vessel elements) in which the voltage source term is zero. The current vector $\delta I^T = [\delta I_c \quad \delta I_v]$ is partitioned accordingly. The symmetric mutual inductance matrix M represents the electrical influence the before mentioned conductors have on one another and the diagonal matrix R represents the resistance of the conductors. The column matrices Ψ_z and Ψ_r are the partial derivatives of the magnetic flux at the conductors, with respect to the vertical (z_C) and radial (r_C) motion of the plasma.

To characterize the plasma position, the centre of the plasma current distribution is used. The vertical coordinate of this plasma current centroid is defined as $z_C = \frac{1}{I_p}\int_{\Omega_p} z J_\varphi dS$, where J_φ is the toroidal current density inside the plasma region Ω_p and I_p is the total plasma current which is assumed to be constant in the derivations of the plasma response model [4].

A. Massless plasma model

In most control analyses, the plasma mass m is neglected for convenience of design. Using (1) the massless model ($m = 0$ model) of the plant dynamics can be written as

$$\dot{I} = -M_*^{-1} R \delta I + M_*^{-1} U \delta V\,, \tag{2}$$

where $M_* = \mathrm{M} + \Psi_r(\partial r_C/\partial I) + \Psi_z(\partial z_C/\partial I)$. The row vectors $\partial r_C/\partial I$ and $\partial z_C/\partial I$ are derived from a linearization of the plasma response around the chosen nominal plasma equilibrium.

B. Plasma with mass model

The plasma with mass model ($m > 0$ model) reflects the reality better than (2), therefore this model will also be referred to as the physical model. For a plasma having mass $m > 0$, perturbations in the vertical motion $\delta z_C = z_C - z_{C,eq}$ can be represented by the inertial momentum equation

$$m\ddot{z}_C = f_z \delta z_C + f_I \delta I\,, \tag{3}$$

where $f_z = \partial F_z/\partial z_C$ is the vertical force produced by the radial field B_R on a plasma subjected to a unit vertical displacement, which is dependent on the magnitude and the degree of curvature of the radial field and the total plasma current I_p. The row matrix $f_I = \partial F_z/\partial I$ contains the vertical forces acting on the plasma, produced by unit currents flowing in the circuits. F_z is the total (scalar) vertical force acting on the plasma. We note that $\Psi_z^T = f_I$ [5][6].

Equation (3) represents a vertical force balance when $\ddot{z}_C = 0$, in which $f_z \delta z_C$ is the destabilizing force (because $f_z > 0$), and $f_I \delta I$ is the stabilizing force. The mass m is assumed to be constant, since the changes in mass are slow relative to the typical time scale considered in the position control design problem. Defining the variables $v_z = \frac{d}{dt}\delta z_C$, and $x_z^T = [v_z \quad \delta z_C]$, we can write (3) as

$$\begin{bmatrix} 0 & 1 \\ m & 0 \end{bmatrix} \dot{x}_z + \begin{bmatrix} -1 & 0 \\ 0 & f_z \end{bmatrix} x_z + \begin{bmatrix} 0 \\ -f_I \end{bmatrix} \delta I = 0. \tag{4}$$

From (1) we obtain

$$M_\# \dot{I} + R\delta I + \Psi_z \dot{z}_C = U\delta V\,,$$

where $M_\# = \mathrm{M} + \Psi_r(\partial r_C/\partial I)$. Combining with (4) and increasing the state dimension by two using $x^T = [v_z \quad \delta z_C \quad \delta I^T]$, we obtain the plasma with mass model

$$\dot{x} = -\tilde{M}^{-1}\tilde{R}x + \tilde{M}^{-1}\tilde{U}\delta V\,, \tag{5a}$$

where

$$\begin{aligned} \tilde{M} &= \begin{bmatrix} 0 & 1 & \boldsymbol{O}_{1xn} \\ m & 0 & \boldsymbol{O}_{1xn} \\ \boldsymbol{O}_{nx1} & \Psi_z & M_\# \end{bmatrix}, \\ \tilde{R} &= \begin{bmatrix} -1 & 0 & \boldsymbol{O}_{1xn} \\ 0 & -f_z & -\Psi_z^T \\ \boldsymbol{O}_{nx1} & \boldsymbol{O}_{nx1} & R \end{bmatrix}, \quad \tilde{U} = \begin{bmatrix} \boldsymbol{O}_{1xn_c} \\ \boldsymbol{O}_{1xn_c} \\ U \end{bmatrix}. \end{aligned} \tag{5b}$$

When $f_z > 0$, the state matrix $A \stackrel{\text{def}}{=} -M_*^{-1}R$ of the massless plasma model and the state matrix $\tilde{A} \stackrel{\text{def}}{=} -\tilde{M}^{-1}\tilde{R}$ of the plasma with mass model both possess a single positive real eigenvalue, which is shown in [1] using a matrix pencil analysis. This positive real eigenvalue is the growth rate γ of the vertical instability. The accompanying eigenvector is a nearly rigid vertical motion of the plasma current distribution.

C. Control Architecture

To stabilize the vertical instability, an additional voltage δV is applied to the control coils, in response to the displacement of δz_C from some reference position $\delta z_{C,ref}$, in the form

$$\delta V(s) = -C(s)\left(\delta z_c(s) - \delta z_{C,ref}(s)\right), \tag{6}$$

where $C(s)$ is the transfer function of the SIMO-controller. The control coils have the additional purpose of controlling the plasma shape and plasma current. However, the control objectives can be performed on different time scales. For most tokamaks the double loop approach shown in Fig. 2 is used. A fast, inner control loop is dedicated to stabilize the vertical instability, most often taking a proportional-derivative (PD) form. Integral action is rarely used, leaving possible steady state errors to the plasma shape controller in the slower, outer loop. These steady state errors are present when no control coils are super conductive, since the system has a finite DC gain in this case.

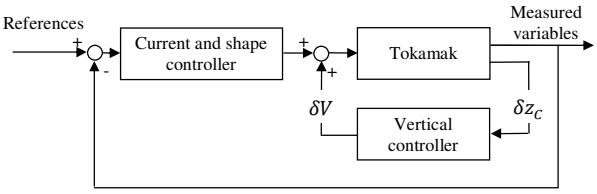

Fig. 2. A simplified scheme of the tokamak feedback system

Often the reference position $\delta z_{C,ref}$ is taken to be zero, making it possible to write the feedback law (6) in the matrix notation

$$\delta V(s) = [O_{n_c x1} \quad -C(s) \quad O_{n_c xn}]x\,. \tag{7}$$

Substituting (7) in the plasma with mass model (5) and replacing the Laplace variable s with λ, results in a matrix $\left(\tilde{M}\lambda + \tilde{R} - \tilde{U}[O_{n_c x1} \quad -C(\lambda) \quad O_{n_c xn}]\right)$ whose determinant

$$\det\begin{pmatrix} -1 & \lambda & O_{1xn} \\ \lambda m & -f_z & -\Psi_z^T \\ O_{nx1} & \Psi_z\lambda + UC(\lambda) & M_{\#}\lambda + R \end{pmatrix} = 0\,, \tag{8}$$

defines the characteristic equation. By adding λ times column one to column two and taking the Laplace expansion along the first row, (9) can be simplified to

$$\det\begin{pmatrix} \lambda^2 m - f_z & -\Psi_z^T \\ \Psi_z\lambda + UC(\lambda) & M_{\#}\lambda + R \end{pmatrix} = 0\,. \tag{9}$$

The system has poles where this characteristic equation vanishes.

III. Theoretical analysis

To obtain an intuitive understanding of the problem, first two low dimensional models are analyzed. The model in section III-B only has a single control coil circuit dedicated to the vertical stabilization task. This model is used to investigate the relation between the high frequency asymptote of a controller and the validity of the $m = 0$ model. The model in section III-C, which also includes a state describing the current in the passive conductors, is used to investigate under what conditions derivative gain is stabilizing for the physical model. In section III-D the general problem is addressed. These theoretical models are related to the single, two and full- circuit experimental models described in section IV.

A. Definitions and nomenclature

Because the two low order models only have one control circuit, the controller in the feedback law (6) can be written as a general SISO LTI-controller $C(s)$ whose transfer function

$$C(s) = \tau_1(s)/\tau_2(s)\,, \tag{10a}$$

is constructed from a ratio between two polynomial transfer functions, expressed in summation form

$$\begin{aligned} \tau_1(s) &= \sum_{p=0}^{n_1} a_p s^{n_1-p}\,,\ a_0 \neq 0\,, \\ \tau_2(s) &= \sum_{p=0}^{n_2} b_p s^{n_2-p}\,,\ b_0 = 1\,, \end{aligned} \tag{10b}$$

where n_1 and n_2 are nonzero, positive integers. The restriction $b_0 = 1$ is for simplicity but without loss of generality (i.e. if $b_0 \neq 1$, rewrite (10) by dividing τ_1 and τ_2 by b_0). All other coefficients a_p, $p = 1,2,\dots,n_1$, and b_p, $p = 1,2,\dots,n_2$, are gains that can arbitrarily be set to zero to construct different controllers forms. Note that $b_p \geq 0, \forall p \in \mathbb{N}$ is a necessary (but not sufficient) condition for having no unstable controller roots.

Definition 3.1

A controller-*form* is a controller obtained from the general form (10) by choosing n_1 and n_2 and arbitrarily setting coefficients to zero. All other gains can take values in $\mathbb{R}$. For instance setting $n_1 = 2$, $n_2 = 1$ and $b_1 = 0$ results in a PID-controller-*form* $C(s) = \frac{a_0 s^2 + a_1 s + a_2}{s}$ with $a_0 \in \mathbb{R}$, $a_1 \in \mathbb{R}$ and $a_2 \in \mathbb{R}$.

A controller-*manifestation* of a controller-form is a controller with a particular set of gain values, for instance the PID-controller-*manifestation* $C(s) = \frac{s^2+2s+3}{s}$. ■

Definition 3.2

A controller-form is said to be *predictive* when asymptotic stability of the closed loop of the physical model (5) is predicted correctly for all possible manifestations of the controller-form, using only a massless plasma analysis (2).

A controller-form is said to be *artifactual* when there exist *manifestations* of this controller-form that asymptotically stabilize (2), but do not stabilize (5). ■

For *predictive* controller-forms, only a massless plasma analysis is sufficient. All manifestations of this form will also stabilize the plasma with mass model when they stabilize the massless plasma model, so automated controller design methods can be used carefree to find appropriate controller gains and parameters.

For controllers that are *artifactual* however, the massless plasma analysis is only usable in combination with *a-priori* knowledge from physical properties. When advanced control techniques are used, a positive mass test that contains this knowledge, like the positivity conditions for PD-controllers in [1], has to be used to detect artifactual behavior due to the massless plasma assumption.

B. Single circuit systems

Define a low dimensional model with only one control circuit, and where no passive structures are present. The matrices $M_\#$, R and the vector $\Psi_z^T = f_I$ reduce to scalars, enabling us to write the scalar characteristic equation using (9)

$$mM_\#\lambda^3 + mR\lambda^2 + (\Psi_z^2 - f_z M_\#)\lambda + \Psi_z C(\lambda) - f_z R = 0 \quad (11)$$

Substituting the general SISO controller form (10) for the controller $C(\lambda)$ into the characteristic equation and multiplying by the controller denominator $\tau_2(\lambda)$ we get

$$\{mM_\#\lambda^3 + mR\lambda^2 + (\Psi_z^2 - f_z M_\#)\lambda - f_z R\}\sum_{p=0}^{n_2} b_p \lambda^{n_2-p} + \Psi_z \sum_{p=0}^{n_1} a_p \lambda^{n_1-p} = 0 \ .$$

After expanding we obtain the characteristic equation in summation form

$$\begin{aligned} &\sum_{p=0}^{n_2} mM_\# b_p \lambda^{n_2+3-p} \\ &+ \sum_{p=1}^{n_2+1} mR b_{p-1} \lambda^{n_2+3-p} \\ &+ \sum_{p=2}^{n_2+2} (\Psi_z^2 - f_z M_\#) b_{p-2} \lambda^{n_2+3-p} \\ &- \sum_{p=3}^{n_2+3} f_z R b_{p-3} \lambda^{n_2+3-p} \\ &+ \sum_{p=3+n_d}^{n_1+3+n_d} \Psi_z a_{p-3-n_d} \lambda^{n_2+3-p} = 0 \, , \end{aligned} \quad (12)$$

where $n_d = n_2 - n_1$ is defined as the relative degree of the controller. The closed loop poles of the single circuit system example are found by setting (12) to zero. All coefficients are strictly real, therefore Descartes' rule of signs [7] provides necessary (but not sufficient) conditions for closed loop stability demanding that all coefficients of (12) have the same sign. Comparing these signs for $m > 0$ and $m = 0$ in (12) reveals some controller properties that are related to the existence of the artifactual behavior (definition 3.2). An interpretation of (12) is provided in the remainder of this section, while making a distinction between (strictly) proper controllers ($n_d \geq 0$) and non-proper controllers ($n_d < 0$).

1) Proper and strictly proper controllers

For all proper and strictly proper controllers, the highest order coefficient in the characteristic polynomial, found by evaluating (12) for $p = 0$, corresponds to λ^{n_2+3} and equals $mM_\#$. For a plasma having mass $m > 0$, $mM_\#$ is strictly positive. For the same sign condition to hold, all other coefficients in (12) also have to be positive, i.e. the leading coefficient puts a positivity constraint on all other coefficients. In the massless plasma analysis, the first two sums in (12) drop out. The highest order coefficient $\Psi_z^2 - f_z M_\#$ is positive when $f_z < \frac{\Psi_z^2}{M_\#}$. The multivariable analogue of this inequality, $f_z < \Psi_z^T M_\#^{-1} \Psi_z$, is characteristic for systems that are not *ideal unstable*. The so called ideal unstable systems have instabilities so fast they cannot be practically feedback stabilized [2]. Ideal instability will be further discussed in section IV-A. When the inequality is satisfied, the 3rd term in (12) is positive, and therefore both (2) and (5) have a positivity constraint on their closed loop characteristic polynomial coefficients.

A set of sufficient conditions can be obtained by application of the Routh-Hurwitz (RH) test [8]. This test also provides a set of coefficients, and requires these to have the same sign. Because the two highest order RH coefficients are always equal to the two highest order coefficients from the polynomial to which the RH test is applied, the sign constraint on the coefficients of the RH test is inherited from the characteristic polynomial coefficients.

The artifactual behavior only occurs when the sign of these coefficients in the $m = 0$ model are all negative while they have sign differences in the $m > 0$ model. Therefore a controller-form (10) is *predictive* for the scalar single circuit model, if the controller satisfies $n_d > 0$ (strictly proper) and the system satisfies $f_z < \frac{\Psi_z^2}{M_\#}$.

2) Non-proper controllers

For non-proper controllers satisfying $-2 \leq n_d \leq -1$, the highest order coefficient $mM_\#$ in (12) puts a positivity constraint on the other coefficients. Setting the mass to zero to obtain the $m = 0$ model is essentially a bifurcation, since the $mM_\#$ coefficient vanishes, and the new highest order coefficient, $\Psi_z^2 - f_z M_\# + \Psi_z a_\mathrm{k}$, (where $k = -1 - \mathrm{n_d}$) contains the gain value $a_\mathrm{k} \in \mathbb{R}$, preventing a sign conclusion (assuming $\Psi_z \neq 0$) since the gain value can adopt all possible values. There could exist a set of gain values for which this coefficient and all other coefficients of the closed loop characteristic polynomial of (12) can become negative, which also satisfies the same sign condition. The negative sign of the two leading coefficients is inherited into the coefficients following from the Routh-Hurwitz test, which also could become negative for these gain values, concluding that the closed loop of the massless plasma model is stable, while the closed loop for a system having a small positive mass is unstable. Hence, these non-proper controllers are artifactual: A controller-form (10) can be *artifactual* for the scalar single circuit model, if it satisfies $-2 \leq n_d \leq -1$, $a_1 \neq 0$, and $b_k \neq 0$, $k = 1,2,\dots,n_2$.

When the controller is highly non-proper, i.e. $n_1 \geq n_2 + 3$, terms with gain values of the numerator are added to the coefficients that were responsible for the positivity constraint in the $m > 0$ model, but that were absent in the $m = 0$ model. They now equal $mM_\# + \Psi_z a_{-3-n_d}$ and $mR + \Psi_z a_{-2-n_d}$ (obtained from the first two sums). When their gain values are nonzero, the positivity constraint caused

by the positive mass in the $m > 0$ model is lost. Setting m to zero in these coefficients does not have a big impact, assuming m to be negligible small, i.e. the mass m is not a bifurcation parameter anymore. Therefore, any artifactual behavior for this set of controllers can be ruled out: A controller-form (10) is *predictive* for the scalar single circuit model, if the controller satisfies $n_d \leq -3$ and $a_k \neq 0$, k=$-3-n_d$, $-2-n_d$.

Example 3.3

To illustrate what happens with an artifactual controller, we choose a controller of the PD-form $C(s) = a_0 s + a_1$, by setting $n_1 = 1$ and $n_2 = 0$ in (10) and (12), to obtain the characteristic polynomial for this controller

$$mM_{\#}\lambda^3 + mR\lambda^2 + (\Psi_z^2 + \Psi_z a_0 - f_z M_{\#})\lambda + \Psi_z a_1 - f_z R = 0 \quad (13)$$

When the derivative gain $a_0 < \frac{f_z}{\Psi_z} M_{\#} - \Psi_z$ and the proportional gain $a_1 < \frac{f_z}{\Psi_z} R$, the sign of the coefficients of the characteristic polynomial of the massless plasma analysis is not consistent with the sign constraint in the $m > 0$ model. This artifactual behavior of the PD-controller is visualized in Fig. 3. The $m > 0$ model has the additional necessary condition $a_0 > \frac{M_{\#}}{R} a_1 - \Psi_z$, which results from the entry $\frac{\Psi_z}{R}(Ra_0 + R\Psi_z - M_{\#}a_1)$ in the Routh-Hurwitz table belonging to (13). ■

C. Two circuit systems

The scalar analysis of section III-A is extended to a system with one circuit for the control coil(s) and one circuit for the passive conductor(s). This system is more representative of the general problem because it has all of the key characteristics. It is used to investigate under what condition derivative gain is stabilizing for the physical model. Therefore, only the $m > 0$ case is considered in this section. Using the notations for this two circuit system

$$\begin{aligned} f_I^T = \Psi_z &= [\Psi_1 \quad \Psi_2]^T, \\ M_{\#} &= \begin{bmatrix} M_{11} & M_{12} \\ M_{12} & M_{22} \end{bmatrix}, \\ R &= \begin{bmatrix} R_1 & 0 \\ 0 & R_2 \end{bmatrix}, \\ U &= [1 \quad 0]^T, \end{aligned} \quad (14)$$

where $|M_{\#}| > 0, R_1 \geq 0$ and $R_2 > 0$, the determinant (9) reduces to the determinant of a 3x3 system

$$\det \begin{pmatrix} \lambda^2 m - f_z & -\Psi_1 & -\Psi_2 \\ \Psi_1\lambda + C(\lambda) & M_{11}\lambda + R_1 & M_{12}\lambda \\ \Psi_2\lambda & M_{12}\lambda & M_{22}\lambda + R_2 \end{pmatrix} = 0\,. \quad (15)$$

1) Pure derivative control

Implementing the pure derivative controller $C(s) = a_0 s$ in (15) yields the characteristic polynomial for the closed loop

$$\begin{aligned} &m|M_{\#}|\lambda^4 \\ &+m(M_{11}R_2 + M_{22}R_1)\lambda^3 \\ &+\{mR_1R_2 + |M_{\#}|(\Psi_z^T M_{\#}^{-1}\Psi_z - f_z) \\ &\quad +a_0(M_{22}\Psi_1 - M_{12}\Psi_2)\}\lambda^2 \\ &+(R_1\Psi_2^2 + R_2\Psi_1^2 - f_z(M_{11}R_2 + M_{22}R_1) + a_0\Psi_1 R_2)\lambda \\ &-R_1R_2f_z = 0\,. \end{aligned} \quad (16)$$

The highest order coefficient $m|M_{\#}|$ in (16) is strictly positive. The lowest order coefficient $-R_1R_2f_z$ is strictly negative when the control coil has a positive resistance. In this case, due to the sign difference between the lowest and highest order coefficient, it is concluded that pure derivative gain is not stabilizing.

When the control coil is super conductive, i.e. $R_1 = 0$, the lowest order coefficient is zero and one root of (15) will consequently be at the origin in the complex plane. The system can be marginally stabilized if and only if there exists a gain a_0 for which the three remaining roots are in the left half plane (LHP) or on the imaginary axis. The first two RH coefficients are equal to the first two coefficients in (16) and therefore strictly positive. None of the poles of (16) are in the RHP iff all RH coefficients are nonnegative. The remaining RH coefficients provide conditions on the derivative gain, $a_0 \leq \frac{M_{11}}{M_{12}}\Psi_2 - \Psi_1$ and $a_0 \geq \frac{M_{11}}{\Psi_1} f_z - \Psi_1$, which will be satisfied iff

$$\frac{\Psi_1\Psi_2}{M_{12}} \geq f_z\,. \quad (17)$$

This inequality will under normal conditions be satisfied for tokamak-plasma models. Thus, pure derivative gain can never asymptotically stabilize the two circuit plasma-coil-vessel model, but it can marginally stabilize the model iff the control coil is super conductive and (17) is satisfied.

2) Proper derivative control

To investigate proper derivative control, the transfer function $C(s) = \frac{a_0 s}{s + b_1}$ is substituted in (15) and the characteristic polynomial is recalculated. The highest coefficient of this polynomial is $m|M_{\#}| > 0$ while the lowest order coefficient equals $-R_1R_2f_zb_1$. The implemented controller is stable by itself, i.e. $b_1 > 0$, and therefore the lowest order coefficient is negative when the control coil has a nonzero electrical resistance. Hence also this proper derivative controller is not asymptotically stabilizing, but marginally stabilizing iff the control coil is super conductive and all RH coefficients are nonnegative. This set of sufficient conditions for marginal stabilization is a rather complicated set of polynomial-in-gain inequalities and very difficult to interpret physically. One such condition,

$$b_1 \leq a_0 \frac{\Psi_1}{(f_z - \Psi_1 M_{11}^{-1}\Psi_1)M_{11}}, \quad (18)$$

is useful however in showing the relative simple relationship between the derivative gain and the location of controller pole $-b_1$ which may not be too far in the LHP.

D. Multi circuit systems

In this section, the tokamak-model has $n = n_c + n_v$ conductors, consisting of n_c control coils and n_v passive structures. All conductors are assumed to be resistive. Again, the general form for SISO controllers (10) is used. This control action is mapped into multiple control coils by multiplying the controller with $U_\#$. This mapping array $U_\#$ of size n_cx1 multiplies the entire SISO controller with a nonzero factor for each active control coil, and with zeros in the case of inactive control coils. To calculate the determinant from the multivariable system matrix (9), a decomposition of the matrix pencil $\lambda M_\# + R$ is necessary. Hereto, define Λ and E as the eigenvalue and eigenvector matrices respectively, in order to satisfy the eigenvalue problem $M_\# E\Lambda + RE = 0$, with the eigenvectors normalized on R, i.e. $E^T RE = I$. Multiplying (9) on the left by $\begin{bmatrix}1 & 0\\ 0 & E^T\end{bmatrix}$ and on the right by $\begin{bmatrix}1 & 0\\ 0 & E\Lambda\end{bmatrix}$ we obtain

$$\det\begin{pmatrix}\lambda^2 m - f_z & -\Psi_z^T E\Lambda\\ E^T\big(\Psi_z\lambda + UU_\# C(\lambda)\big) & \lambda E^T M_\# E\Lambda + E^T RE\Lambda\end{pmatrix} = 0\,.$$

Using that $M_\#$ is positive definite and symmetric and R is diagonal (known from physical principles [5]), and defining the objects $\xi = E^T\Psi_z$ and $\Delta = E^T UU_\#$ the determinant is simplified to

$$\det\begin{pmatrix}\lambda^2 m - f_z & -\xi^T\Lambda\\ \xi\lambda + \Delta C(\lambda) & \Lambda - \lambda I\end{pmatrix} = 0\,,$$

and further simplified using a block matrix calculation to

$$\det(\Lambda - \lambda I)\det\Big(\lambda^2 m - f_z + \xi^T\Lambda(\Lambda - \lambda I)^{-1}\big(\xi\lambda + \Delta C(\lambda)\big)\Big) = 0\,.$$

After expanding this product, the determinant is given by the expression

$$(\lambda^2 m - f_z)\prod_{\mathrm{i}=1}^{\mathrm{n}}(\lambda_\mathrm{i} - \lambda) + \sum_{k=1}^{n}\lambda_k\left(\xi_k^2\lambda + \xi_k\Delta_k C(\lambda)\right)\prod_{\substack{\mathrm{i}=1\\ \mathrm{i}\neq\mathrm{k}}}^{\mathrm{n}}(\lambda_\mathrm{i} - \lambda) = 0\,,$$

which contains products that are expanded using the identities

$$\prod_{\mathrm{i}=1}^{\mathrm{n}}(\lambda_\mathrm{i} - \lambda) = (-1)^{\mathrm{n}}\sum_{\mathrm{k}=0}^{\mathrm{n}}\lambda^{\mathrm{n}-\mathrm{k}}\mathrm{s}_\mathrm{k}\,,$$
$$\prod_{\substack{\mathrm{i}=1\\ \mathrm{i}\neq\mathrm{k}}}^{\mathrm{n}}(\lambda_\mathrm{i} - \lambda) = (-1)^{\mathrm{n}+1}\sum_{\mathrm{k}=1}^{\mathrm{n}}\lambda^{\mathrm{n}-\mathrm{k}}\mathrm{s}_{\mathrm{k}-1,\mathrm{i}-}\,,$$

where s_k is defined as the sum of products of the eigenvalues λ_k of the pencil $\lambda M_\# + R$ taken k at a time, multiplied by $(-1)^k$, e.g. $s_1 = -\sum_{\mathrm{k}=1}^{\mathrm{n}}\lambda_\mathrm{k}$, $s_2 = \sum_{\substack{j,k=1\\ j<k}}^{n}\lambda_j\lambda_k$, $s_n = (-1)^n\sum_{k=1}^{n}\lambda_k$ and $s_0 \overset{\text{def}}{=} 1$. Note that $s_k > 0, \forall k \in \mathbb{N}$ since all eigenvalues of $\lambda M_\# + R$ are strictly negative [1].

Substituting the identities into the characteristic polynomial and omitting the sign $(-1)^n$ of the polynomial, we obtain

$$(\lambda^2 m - f_z)\sum_{k=0}^{n}\lambda^{n-k}s_k + \sum_{k=1}^{n}\lambda^{n-k}(\lambda\xi^T + C(\lambda)\Delta^{\mathrm{T}})P_{k-1}\xi = 0\,,$$

where $P_k = -\Lambda\,\mathrm{diag}\{s_{k,1-}\quad s_{k,2-}\quad\cdots\quad s_{k,n-}\}$ is built from the objects $s_{k,i-}$ that are based on the objects s_k, but with eigenvalue λ_i removed, and $s_{0,i-} \overset{\text{def}}{=} 1$. We note that $P_0 = -\Lambda$, $P_{n-1} = s_n I$ and $P_k > 0, \forall k \in \mathbb{N}$.

Expanding and multiplying the polynomial by the controller denominator $\tau_2(\lambda)$ results in

$$\lambda^2 m\sum_{k=0}^{n}\lambda^{n-k}s_k\tau_2(\lambda) - f_z\sum_{k=0}^{n}\lambda^{n-k}s_k\,\tau_2(\lambda) + \sum_{k=1}^{n}\lambda^{n-k}\lambda\xi^T P_{k-1}\xi\tau_2(\lambda) + \sum_{k=1}^{n}\lambda^{n-k}\,\Delta^{\mathrm{T}}P_{k-1}\xi\,\tau_1(\lambda) = 0\,.$$

After inserting the controller polynomials and equalizing all powers of λ, the resulting closed loop characteristic polynomial of the multivariable plasma-coil-vessel model is

$$\begin{aligned} &m\sum_{k=0}^{n}\sum_{p=0}^{n_2}\lambda^{n+n_2+2-p-k}b_p s_k\\ &-f_z\sum_{k=2}^{n+2}\sum_{p=0}^{n_2}\lambda^{n+n_2+2-p-k}b_p s_{k-2}\\ &+\sum_{k=2}^{n+1}\sum_{p=0}^{n_2}\lambda^{n+n_2+2-p-k}b_p\xi^T P_{k-2}\xi\\ &+\sum_{k=3+n_d}^{n+2+n_d}\sum_{p=0}^{n_1}\lambda^{n+n_2+2-p-k}\,\Delta^{\mathrm{T}}a_p P_{k-3-n_d}\xi = 0\,. \end{aligned} \tag{19}$$

Note that this polynomial-in-gains consists of scalar coefficients. It is easily seen that the only difference between the $m = 0$ and the $m > 0$ model is contained in the first line. When the relative degree of the controller $n_d \geq -2$, the leading coefficient in (19) for the $m > 0$ model, is found by evaluating the double sum on the first line for $(k, p) = (0,0)$. This coefficient, corresponding to λ^{n+n_2+2} equals $mb_0 s_0 = m > 0$ since $b_0 = 1$ and $s_0 = 1$ by definition. For the $m = 0$ model, the highest coefficient in the case of $n_d \geq 0$ equals $-f_z - \xi^T\Lambda\xi = -f_z - \Psi_z^T E\Lambda E^T\Psi_z = -f_z + \Psi_z^T M_\#^{-1}\Psi_z$ which is larger than zero for systems that are not ideal unstable. Therefore, for strictly proper controllers, due to the positivity constraint provided by the leading coefficient, both the $m = 0$ and the $m > 0$ model require all

coefficients of (19) to be positive in order to satisfy Descartes' rule of signs. No set of gains exists that can make all coefficients of (19) negative for the $m = 0$ model, concluding that strictly proper controllers are predictive for model (19). In Table 1 an overview is provided of the leading coefficient of (19) for different cases of the controller's relative degree. The same behavior as described in III-B is recognized.

Table 1: Highest order coefficient from (19)

n_d	$m > 0$ model	$m = 0$ model	Predictive
> 0	m	$-f_z - \xi^T \Lambda \xi$	Yes[1]
0	m	$-f_z - \xi^T \Lambda \xi$	Undetermined[2]
-1		$-f_z - (\xi + a_0 \Delta)^T \Lambda \xi$	Undetermined[2]
-2		$-a_0 \Delta^T \Lambda \xi$	Undetermined[2]
-3	$m - a_0 \Delta^T \Lambda \xi$		Yes[3]
≤ -4	$-a_0 \Delta^T \Lambda \xi$		Yes[3]

[1] Assuming the system is not ideal unstable, i.e. $\Psi_z^T M_\#^{-1} \Psi_z > f_z$

[2] The controller can be either artifactual or predictive

[3] Assuming m is negligible small and requiring that $a_{-3-n_d} \neq 0$

For controllers satisfying $n_d \leq -3$ the artifactual behavior is prevented since the term that was responsible for the positivity constraint in the $m > 0$ model and that was absent in the $m = 0$ model, now equals $m - a_{-3-n_d} \Delta^T \Lambda \xi$ and hence, m is not a bifurcation parameter anymore: A controller-form (10) is predictive for the multi circuit model (19), if the controller satisfies $n_d \geq 0$ and the model satisfies $\Psi_z^T M_\#^{-1} \Psi_z > f_z$ or when the controller satisfies $n_d \leq -3$ and $a_{-3-n_d} \neq 0$.

The lowest order coefficient follows from evaluating the second sum in (19) for $(p, k) = (n_2, n + 2)$ and the fourth sum for $(p, k) = (n_1, n + 2 + n_d)$ and equals $a_{n_1} \Delta^T P_{n-1} \xi - f_z b_{n_2} s_n = \left(a_{n_1} \Delta^T \xi - f_z b_{n_2}\right) s_n$ which should be positive for an asymptotically stable closed loop (assuming $n_d \geq -2$). From this we derive a necessary condition

$$a_{n_1} \Delta^T \xi > f_z b_{n_2} ,$$

that describes the relation between the lowest order controller coefficients. All multiplication factors in $U_\#$ corresponding to control coils positioned above (below) the plasma will be chosen positive (negative). The same holds for the entries of Ψ_z, which are positive (negative) for conductors above (below) the plasma, since positive z refers to an upward perturbation in the position of the plasma. Therefore the product $\Delta^T \xi = (UU_\#)^T R^{-1} \Psi_z$ is strictly positive. For derivative controllers, the gain a_{n_1} is zero, and therefore these controller forms cannot asymptotically stabilize the system with all conductors having a positive electrical resistance.

IV. Simulation Results

Simulations are performed on dynamic models for tokamak and plasma poloidal field systems, generated using a collection of MATLAB functions and scripts, known collectively as TokSys. [9]. More extensive simulation results belonging to this analysis are documented in [10].

A. Single circuit model of KSTAR

For this testcase we take a simple model of the KSTAR tokamak. All control coils and passive stabilizing structures are removed from the full model (Fig. 1), except for the internal control coils ICVU and ICVL that are connected in anti-series to the same power supply, hence (2) has one state and (5) has three states. This model corresponds to the single circuit system analyzed in III-B. The vertical force $f_z \approx 4 \cdot 10^6 \, Nm^{-1}$ elongates the plasma, introducing the vertical instability. No passive conductors are present that can reduce the growth time of this instability. When the system is analyzed using the model that uses a small positive mass (5), the growth rate $\gamma \approx 8.2 \cdot 10^5 \, rad/s$. The massless plasma analysis results in a growth rate of $\gamma \approx -21 \, rad/s$, declaring the open loop (incorrectly) to be stable. This behavior is characteristic of systems having $f_z > \Psi_z^T M_\#^{-1} \Psi_z$ [2]. These so called *ideal unstable* systems have instabilities so fast they cannot be feedback stabilized. Therefore for this first testcase the control coils are moved slightly inwards. Putting them closer to the plasma provides more passive stabilization, resulting in a growth rate of $\gamma \approx 4.12 \, rad \, s^{-1}$ for both the plasma with mass and the massless plasma model; the system is not ideal unstable anymore.

1) PD-controller

A PD-controller $C(s) = a_0 s + a_1$ is used as prototype. The closed loop stability is analyzed for a range of proportional gain values a_1 and derivative gain values a_0.

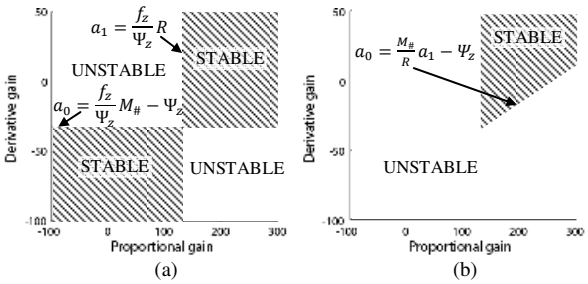

Fig. 3. Indication of stable closed loop ($\gamma_{CL} < 0$) and unstable closed loop ($\gamma_{CL} > 0$) areas for a PD-controller for the massless plasma model (a) and the plasma with mass model (b).

The stability boundaries on these gain values (see Fig. 3) agree with the conditions found in example 3.3.

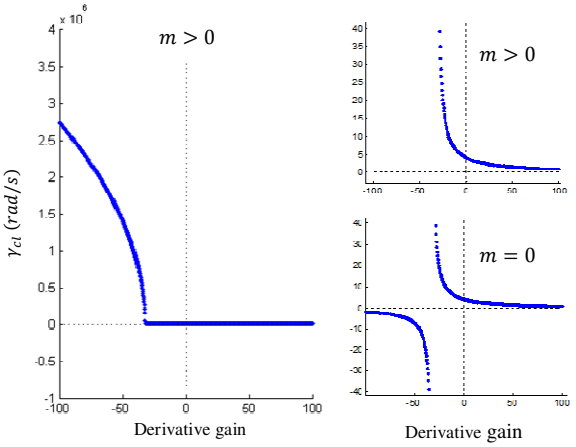

Fig. 4. Closed loop growth rate γ_{CL} of the single circuit model, as a function of derivative gain (zero proportional gain). The growth rate of the $m > 0$ model becomes negative when the derivative gain decreases below -32, whereas the $m > 0$ model becomes more unstable.

Setting the proportional gain to zero, the closed loop growth rate is investigated against varying derivative gain (see Fig. 4). The $m = 0$ model has an artifactual branch for derivative gain sufficiently negative. This result confirms the findings of section III-B2.

1) D-controllers with high frequency roll off

When using a proper controller of the form $C(s) = \frac{a_0 s}{s+b_1}$ this single circuit model (2) and (5) cannot be marginally stabilized. When the pole of this controller is placed at a high frequency, this controller acts as a pure derivative controller on the normal frequency band. Since the controller is proper, the artifactual branch is not present. Similar results are obtained using the strictly proper controller-form $C(s) = \frac{a_0 s}{s^2+b_1 s+b_2}$ with two high frequency poles. This result confirms the findings of section III-B1.

B.

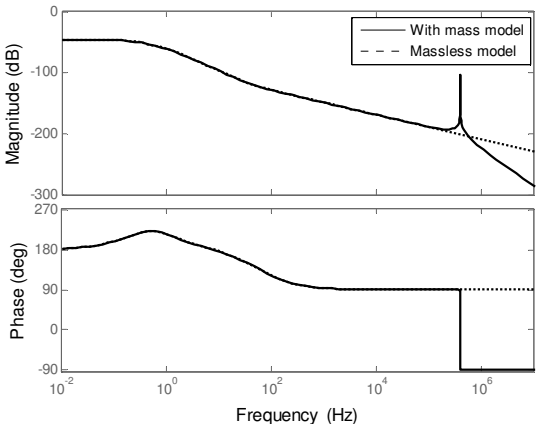

Fig. 5. Bode plot of the with mass model and massless model

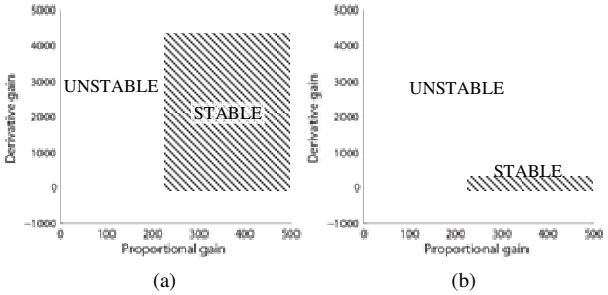

Fig. 6. Indication of stable closed loop ($\gamma_{CL} < 0$) and unstable closed loop ($\gamma_{CL} > 0$) areas for a PD-controller for the massless plasma model (a) and the plasma with mass model (b) of the full KSTAR model. Not visible in this picture is the upper limit on the proportional gain (around 1.6E5) for the stable region.

Full KSTAR model

In the full KSTAR model (Fig. 1) all structures are modeled. The model consists of 103 circuits, built from 86 passive conductors, 16 inactive control coils and the in anti-series connected control coils ICVU and ICVL to the power source (in this case the mapping array $U_{\#}$ from section III-D would have a $+1$ entry corresponding to ICVU and a -1

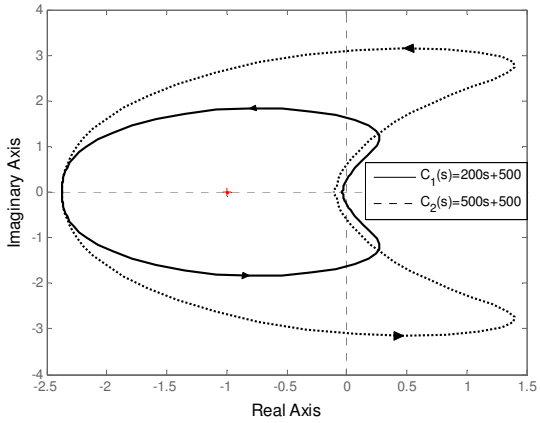

Fig. 7. Nyquist plot of the $m = 0$ model. Both C_1 and C_2 stabilize the system because the Nyquist diagram encircles the -1 point counter clockwise to compensate for the RHP-pole.

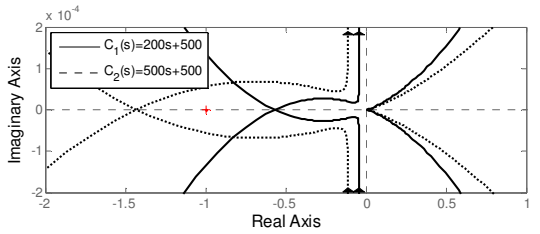

Fig. 8. Nyquist plot of the $m > 0$ model. The undamped resonance causes a big circle in Nyquist that crosses the negative real axis. For C_1, this crossing is to the right of the -1 point so that it is counter clockwise encircled. Increasing the derivative gain stretches the circle along the real axis, and thus moves the crossing to the left of the -1 point. Therefore C_2 does not stabilize the closed loop.

entry corresponding to ICVL). The plasma with mass model and the massless plasma model are compared in Fig. 5. The $m > 0$ model has a high frequency resonance due to the additional pole pair from the inertial momentum equation. Both models have a growth rate of $\gamma \approx 1.46\, rad/s$. Because the RHP-zero ($303\, rad/s$) is sufficiently faster than the RHP-pole ($1.46\, rad/s$), a controller can be designed with an acceptable phase margin. For instance the controller $C_1(s) = 200s + 500$ achieves a bandwidth of $8.3\, rad/s$ which is faster than the RHP-pole, and slower than the RHP-zero. The regions of closed loop stability are analyzed for this high order model, and displayed in Fig. 6. The stable region of the $m = 0$ model is much larger than the stable region of the $m > 0$ model. When the derivative gain is increased above 349, for instance with $C_2 = 500s + 500$, the $m > 0$ closed loop becomes unstable, while the $m = 0$ closed loop remains stable. The discrepancy between the models is explained using Nyquist plots (Fig. 7 and 8).

V. Conclusion

The difference between (2) and (5) is caused by small perturbations in the bifurcation parameter m, that sometimes results in totally different closed loop behavior. In the theoretical section the closed loop characteristic polynomials of three different systems were established. These all showed that this difference can be related to the relative degree of the controller. Erroneous conclusions about marginal stability only happen when the controller is non-proper, with the degree of the numerator one or two orders higher than the degree of the denominator. So only in these cases care has to be taken when the massless model is used to predict stability of the physical model.

To address the question whether velocity feedback will ever stabilize the physical system, three different controllers were evaluated. It turns out that neither the pure derivative controller, nor the proper or strictly proper derivative controller can asymptotically stabilize the physical system. Marginal stabilization is possible, but if and only if all control coils are super conductive.

In the simulation section a complete set of testcases was used. The single circuit model, the two circuit model and the full circuit model from the theoretical section were evaluated using models from KSTAR and ITER. The strictly proper controller was predictive in all testcases. The proper controller was predictive in all testcases where control coils with positive electrical resistance were used, but showed artifactual behavior in some cases with super conductive control coils. In section III-C-2 the two circuit model was addressed. By application of the Routh-Hurwitz test a set of polynomial-in-gains inequalities was established for the proper derivative controller. A simplification of these expressions is needed to formulate under what conditions this controller can marginally stabilize the physical system. A similar set of complex conditions was found by implementing the strictly proper derivative controller, and these also need simplification and interpretation.

A set of easy to check necessary and sufficient conditions for stabilization of the general model, like the positive mass test in [1], could be developed for other, more complex controllers.

Acknowledgment

We gratefully acknowledge the National Fusion Research Institute of Korea for allowing us to use models of the KSTAR Tokamak for the practical examples.

References

[1] M. L. Walker and D. A. Humphreys, *On Feedback Stabilization of the Tokamak Plasma Vertical Instability*, Automatica, vol. 45, no. 3, p.665-674, 2009.

[2] J. William Helton, Kevin J. McGown, M.L. Walker, *Conditions for Stabilization of the Tokamak Plasma Vertical Instability Using Only a Massless Plasma Analysis.* Accepted for publication.

[3] M. L. Walker and D.A. Humphreys (2006a), *A multivariable analysis of the plasma vertical instability in tokamaks*. In Proceedings of the 45th IEEE conference on decision and control, p. 2213.

[4] M. Ariola and A. Pironti. *Magnetic Control of Tokamak Plasmas*. Springer, 2008.

[5] M. L. Walker, D. A. Humphreys, *Valid coordinate systems for linearized plasma shape response models in tokamaks*, Fusion Science and Technology, vol. 50, no. 4, Nov. 2006.

[6] G. Ambrosino and R. Albanese, *Magnetic control of plasma current, position, and shape in tokamaks*, IEEE Control Syst. Mag., vol. 25, no. 5, p. 76-92, Oct. 2005.

[7] R. Descartes, *The Geometry of Rene Descartes with a facsimile of the first edition, translated by D. E. Smith and M.L. Latham*, New York, Dover Publications, 1954.

[8] E.J. Routh, *A Treatise on the Stability of a Given State of Motion*, London: Macmillan and Co., 1877.

[9] D.A. Humphreys, J.R. Ferron, M. Bakhtiari, J.A. Blair, Y. In, G.L. Jackson, H. Jhang, R.D. Johnson, J.S. Kim, R.J. LaHaye, J.A. Leuer, B.G. Penaflor, E. Schuster, M.L.Walker, H. Wang, A.S.Welander and D.G. Whyte, *Development of ITER-relevant plasma control solutions at DIII-D*, Nuclear Fusion, vol. 47, no. 8, p. 943-51, Aug. 2007.

[10] M.J. Beelen, *Stability analysis of velocity feedback for the plasma vertical instability in fusion tokamaks - Simulation result*s. Internal document, General Atomics, San Diego.

[11] G. Ambrosino, M. Ariola, G. De Tommasi, A. Pironti, A. Portone, *Plasma position and shape control in ITER using in-vessel coils*. In Proceedings of the 47th IEEE Conference on Decision and Control, p. 3139.

[12] IEEE Control Systems Magazine, special issue on Control of Tokamak Plasmas, vol. 25, no. 5, Oct. 2005.

[13] IEEE Control Systems Magazine, special issue on Control of Tokamak Plasmas II, vol. 26, no. 2, Apr. 2006.

Stability analysis of velocity feedback for the plasma vertical instability in fusion tokamaks

Simulation Results

M.J. Beelen

***Abstract*— The discrepancy between the massless plasma model and the plasma with mass model, with respect to the vertical instability, is investigated using simulations. These simulations are performed on tokamak and plasma poloidal field models of KSTAR and ITER, with varying magnitudes of instability, including the possibility of super conductive control coils. Also stabilization using velocity feedback is investigated. The results confirm that neither pure velocity feedback nor a proper of strictly proper form of velocity feedback can asymptotically stabilize the vertical instability. This document is inextricably linked to [1].**

I. SIMULATION NOMENCLATURE

To investigate the plasma vertical instability, simulations are performed on dynamic models for tokamak and plasma poloidal field systems, generated using a collection of MATLAB functions and scripts, known collectively as TokSys [2].

The most unstable eigenvalue is used to characterize stability, which is the growth rate γ for the tokamak plasma system, and the growth rate γ_{CL} for the closed loop system. The purpose of the simulations is to compare two models, the plasma with mass model ($m > 0$ model) and the massless plasma model ($m = 0$ model). The $m > 0$ model (equation (2) in [1]), assumes the plasma has a small positive mass and consists of the circuit equations and a second order inertial momentum equation, while the $m = 0$ model (equation (5) in [1]), assumes the plasma is massless and consists of only the circuit equations. Because the $m > 0$ model reflects the reality better, this model will also be referred to as the physical model.

To stabilize the vertical instability, an additional voltage δV is applied to the control coils, in response to the displacement of δz_C from some reference position $\delta z_{C,ref}$, in the form

$$\delta V(s) = -C(s)\left(\delta z_c(s) - \delta z_{C,ref}(s)\right), \tag{1}$$

where $C(s)$ is the transfer function of the SIMO-controller. Four different controller forms are defined to investigate stability of the closed loop. A proportional - derivative (PD) controller C_1, a pure derivative controller C_2, a proper derivative controller C_3, with one pole far in LHP and a strictly proper derivative controller, with two poles placed far in LHP (at locations $-\frac{1}{2}G_2$ and $-\frac{3}{2}G_2$):

$$\begin{aligned} C_1(s) &= G_1 s + G_2\,, \\ C_2(s) &= G_1 s\,, \\ C_3(s) &= G_1 \frac{s}{s+G_2}\,, & G_2 > 0\,, \\ C_4(s) &= G_1 \frac{s}{s^2 + 2G_2 s + \frac{3}{4}G_2^2}\,, & G_2 > 0\,. \end{aligned} \tag{2}$$

These controllers contain one or two gain vectors which map the scalar error of the vertical position to the active control coils. These gains are varied over a wide range to investigate the performance of the controller forms, and to check whether the positive mass test is satisfied. The positive mass test is derived in [3]. It provides necessary and sufficient conditions for a massless plasma analysis to predict the vertical stability of a plasma with small mass:

Positive Mass Test

Consider the tokamak plasma system with a controller (2) rewritten in the form $C(s) = G_d s + G_p + D(s)$ where $D(s)$ is a strictly proper rational function. Suppose the controller asymptotically stabilizes a massless plasma. The equivalent plasma with small positive mass is also asymptotically stabilized **if and only if** the following inequalities hold:

$$\xi = -f_z + f_l M_\#^{-1}[\Psi_z + g_d] > 0$$
$$\eta = f_l M_\#^{-1} g_p - f_l M_\#^{-1} R M_\#^{-1}[\Psi_z + g_d] < 0 \quad (3)$$

■

The lower case g_d and g_p are controller gain vectors that are defined to contain zeros in entries corresponding to the passive (vessel) conductors and are equal to G_d and G_p in entries corresponding to the active control coils. Note that rewriting C_3 in the form results in $G_p = G_1$ and $G_d = 0$. Rewriting C_4 results in $G_p = 0$ and $G_d = 0$.

To classify the properties of a controller, different sets are defined to which a controller can belong. A notation with three subscripts is used. The first subscript is the sign of γ_{cl} for the $m = 0$ model and the second subscript is the sign of γ_{cl} of the $m > 0$ model. This sign can be negative, zero or positive, corresponding to an asymptotically stable, a marginally stable and an unstable system respectively. The third subscript will be an s or an n, denoting whether the positive mass test is **s**atisfied or **n**ot satisfied respectively, see table 1. *Remark: In the sequel, when only the word 'stability' is used, it will denote asymptotic stability. When marginal stability is meant, this will be mentioned explicitly.*

Table 1: Definition of controller sets

		Positive mass test satisfied			Positive mass test not satisfied		
		$m > 0$ model			$m > 0$ model		
		$\gamma_{cl} < 0$	$\gamma_{cl} = 0$	$\gamma_{cl} > 0$	$\gamma_{cl} < 0$	$\gamma_{cl} = 0$	$\gamma_{cl} > 0$
$m = 0$ model	$\gamma_{cl} < 0$	χ_{--s}	χ_{-0s}	χ_{-+s}	χ_{--n}	χ_{-0n}	χ_{-+n}
	$\gamma_{cl} = 0$	χ_{0-s}	χ_{00s}	χ_{0+s}	χ_{0-n}	χ_{00n}	χ_{0+n}
	$\gamma_{cl} > 0$	χ_{+-s}	χ_{+0s}	χ_{++s}	χ_{+-n}	χ_{+0n}	χ_{++n}

E.g. controllers that are designed to stabilize the massless plasma model and that are predictive for the physical model, belong to set χ_{--s}. Controllers that belong to set χ_{-+n} stabilize the $m = 0$ model, but do not stabilize the $m > 0$ model. These are the erroneous controllers that have to be disregarded using the positive mass test. The grey shading in the table marks the sets for which can be reasoned on beforehand that no controllers will belong to these sets in the simulation results. Directly from the positive mass test it follows that set χ_{-0s} and set χ_{-+s} will not exist because when a controller asymptotically stabilizes the $m = 0$ model and the positive mass test is satisfied, the $m > 0$ model will also be asymptotically stabilized. Because of the if and only if condition, the reverse of the positive mass test is also true; when the positive mass test is not satisfied, and the $m = 0$ is stabilized, it can be ruled out that the $m > 0$ is stabilized, hence no controllers can belong to set χ_{--n} or χ_{-0n}. Controllers belonging to sets χ_{+-n} and χ_{0-n} cannot exist because when the $m > 0$ model is stabilized, the positivity conditions always hold (Corollary 1 in [4]).

The main purpose of the simulations is to answer the following questions for different tokamak plasma systems:

1. For what controllers is stability of the physical system correctly predicted when using only the $m = 0$ model? i.e. what controllers are *predictive* or *artifactual?* (See definition 3.2 in [1])
2. Under what conditions can velocity feedback stabilize the physical system?

Velocity feedback can be represented using the pure derivative controller C_2 but also using the proper and strictly proper derivative controller, C_3 and C_4 respectively. When C_3 and C_4 have poles very far in LHP, they act as a derivative controller on the normal frequency band while their roll off is at a much higher frequency.

To obtain a complete set of testcases, three models of KSTAR, called A1, C1 and F1 (see fig. 1), and three models of ITER, called A2, C2 and F2 (see fig. 2) are used. Model F1 and F2 are the full, unreduced models of these tokamaks, containing all passive vessel elements and control coils (corresponding to the theoretical analysis in [1] section III-D). This results in a 103 circuit model for KSTAR, consisting of 86 vessel elements and 18 control coils, of which ICVU and ICVL are connected to the same power source, in anti-series. Therefore the $m = 0$ model of F1 has 103 states, and the $m > 0$ model has 105 states because the inertial momentum equations increase the state dimension by two. The full ITER model has

13 circuits devoted to the control coils and 113 circuits for the passive structures.

The lower order models, C1, C2, A1 and A2, are reduced models, based on the full model but with some circuits omitted or grouped. In models C1 and C2 the vacuum vessel acts as one circuit, i.e. the upper half and lower half of the vessel elements are grouped and connected in anti-series. The second circuit in these models consists of one upper and one lower control coil that are connected in anti-series (corresponding to the model described in [1] section III-C). Models A1 and A2 are single circuit models, where the entire vacuum vessel is also removed, remaining only with the two active internal control coils (see also section III-B in [1]).

The output from simulations on other testcases like B1, B2, D1, D2, E1 and E2, which are also reduced tokamak models, is omitted in this report because the before mentioned testcases already provide a complete set of testcases. These extra testcases were used to validate the other simulations.

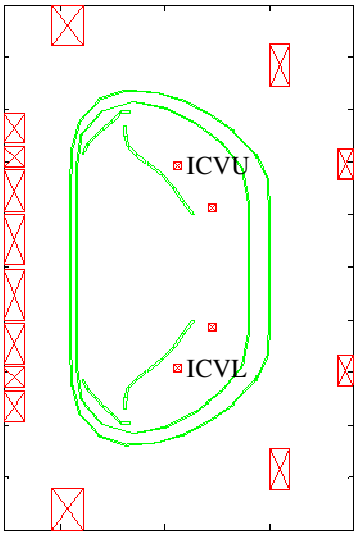

a) Model F1. Full 103 circuit model of KSTAR

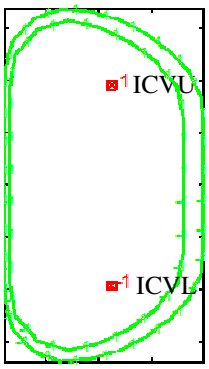

b) Model C1. Two circuit model of KSTAR

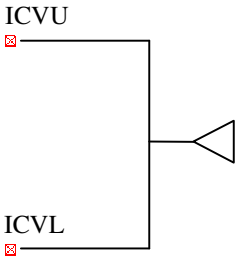

c) Model A1. One circuit model of KSTAR Two internal control coils are connected to the same power source

Fig. 1. KSTAR models used in TokSys

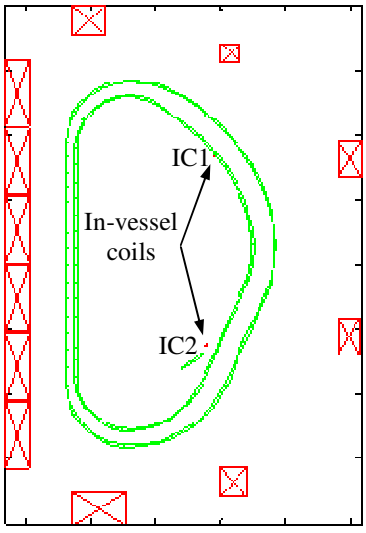

a) Model F2. Full 126 circuit model of ITER

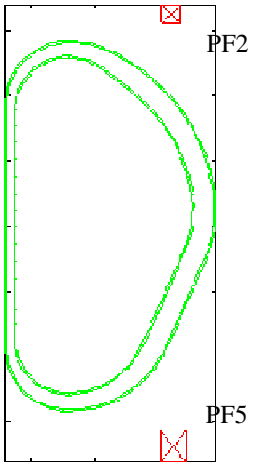

b) Model C2. Two circuit model of ITER

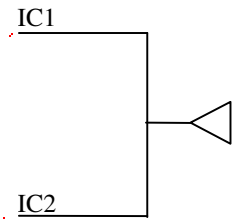

c) Model A2. One circuit model of ITER

Fig. 2. ITER models used in TokSys

II. SIMULATION RESULTS

A. *Testcase A1*

1) Controller C_1

The results obtained from the first testcase using tokamak model A1 and controller C_1 are displayed in fig. 3, for both the $m = 0$ model and the $m > 0$ model. The gains are varied over a wide range, and the closed loop eigenvalues are calculated. A blue dot indicates stability of the closed loop, i.e. $\gamma_{cl} < 0$, whereas a red x-mark denotes $\gamma_{cl} > 0$. Fig. 3c contains the results from the positive mass test.

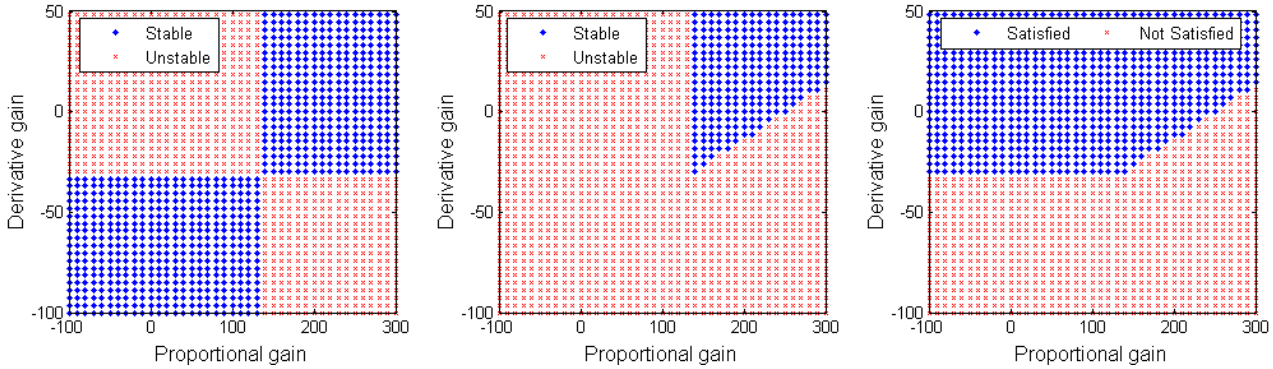

a) $m = 0$ model b) $m > 0$ model c) Positive mass test

Fig. 3. Testcase A1 with controller C_1

Overlaying the contours of the above figures and distinguishing the various controller sets results in Fig. 4.

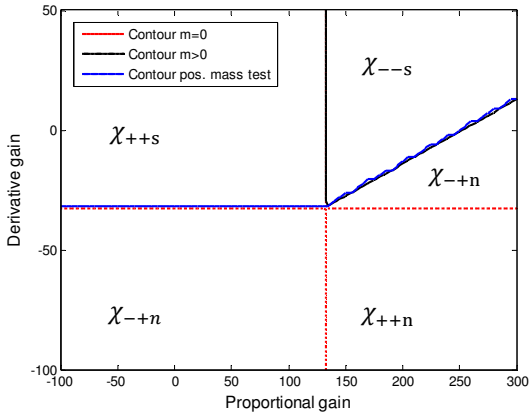

Fig. 4. Indication of sets belonging to testcase A1

Observations:

- The set of gain values that stabilizes the $m = 0$ model is much larger than the set of gain values that stabilizes the $m > 0$ model. Also set χ_{+-s} does not appear. It seems that the $m > 0$ model is stricter than the $m = 0$ model.
- For all gain values that stabilize the $m = 0$ model and do not stabilize the $m > 0$ model, the positive mass test is not satisfied, so these values belong to set χ_{-+n}. The result confirms the validity of the positive mass test.
- Set χ_{++s} exists. So even though the positive mass test is satisfied, both models are not stabilized.

The diagonal matrix R_{pf} represents the resistance of the conductors, corresponding only to the (PF) control coils. The reduced resistance matrix R_{pf}^* is obtained by scaling the original resistance of the control coils using a factor between zero and one. When R_{pf}^* is a zero matrix, the control coils are super conductive. Fig. 5 displays what happens with the sets when this factor is decreased from zero to one.

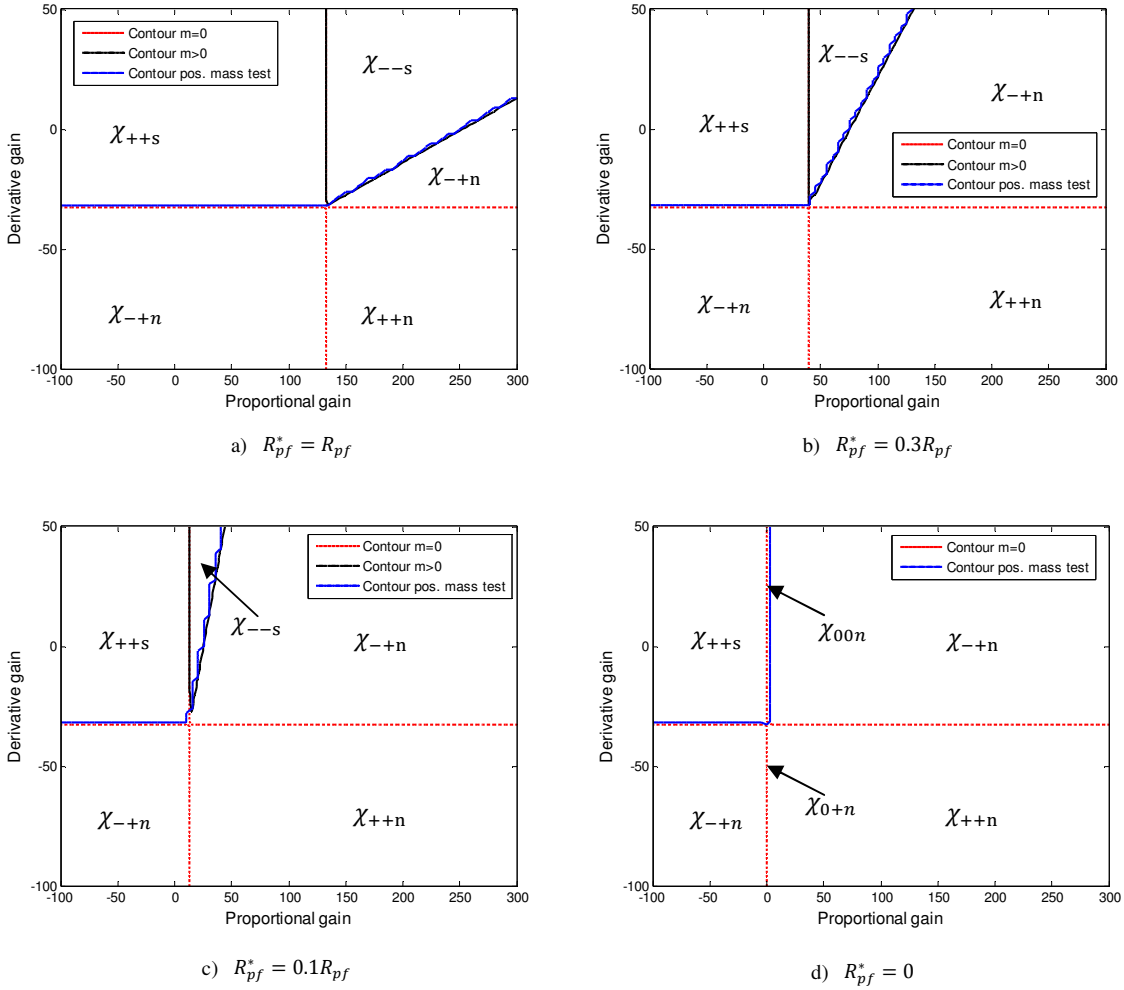

a) $R_{pf}^* = R_{pf}$

b) $R_{pf}^* = 0.3R_{pf}$

c) $R_{pf}^* = 0.1R_{pf}$

d) $R_{pf}^* = 0$

Fig. 5. Decreasing the control coil resistance for testcase A1

- In fig. 5d, where the control coil is super conductive, set χ_{--s} is absent. The physical system is not asymptotically stabilizable anymore using the PD controller.
- The positive mass test in the super conductive case is not valid, since $\eta = 0$, as can be seen in (3xx), by setting $G_p = 0$ and $R = 0$.

2) Controller C_2

- On the line of zero proportional gain, sets χ_{00n} and χ_{0+n} appear. This means that when the control coil in this single conductor system is super conductive, pure derivative gain marginally stabilizes the $m = 0$ model. When $G_d > -32$, it also marginally stabilizes the $m > 0$ model.
- When the single control coil has positive electrical resistance, pure derivative gain cannot stabilize the physical model, see also fig. 5 in [1].

3) Controller C_3

For the case with a control coil that has a positive resistance, the proper derivative controller cannot stabilize the system, but for the case of a super conductive control coil, the system can be marginally stabilized, see fig. 6. Marginal stability, $\gamma_{cl} = 0$, is denoted by a black dot.

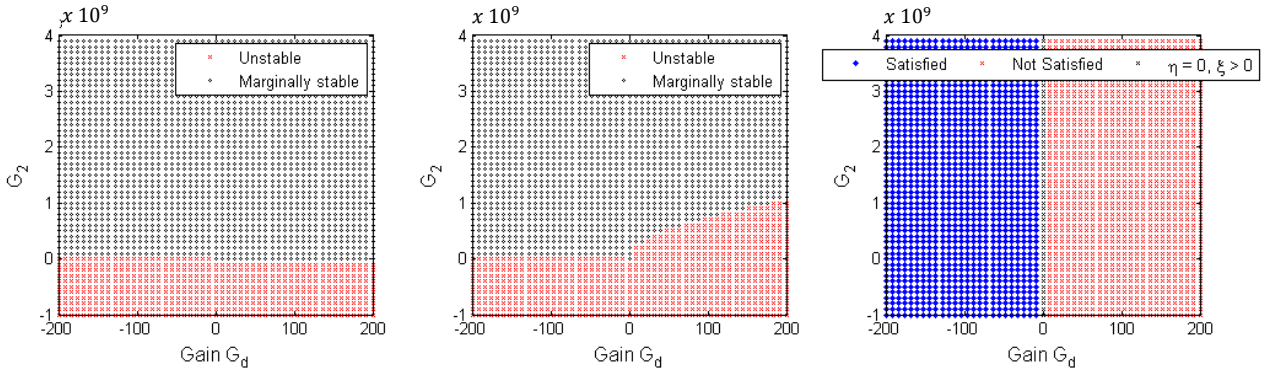

a) $m = 0$ model b) $m > 0$ model c) Positive mass test

Fig. 6. Testcase A1 with controller C_3
Control coil super conductive

- Fig. 6 shows that the C_3 can marginally stabilize both models when the control coil is super conductive.
- Sets χ_{++s}, χ_{00s}, χ_{++n}, χ_{00n} and χ_{0+n} are present.
- For controller C_3, the results of the positive mass test are only dependant on the gain G_d.
- The vertical axis corresponds to the negative of the controller pole, and this position is varied over a wide range.

4) Controller C_4

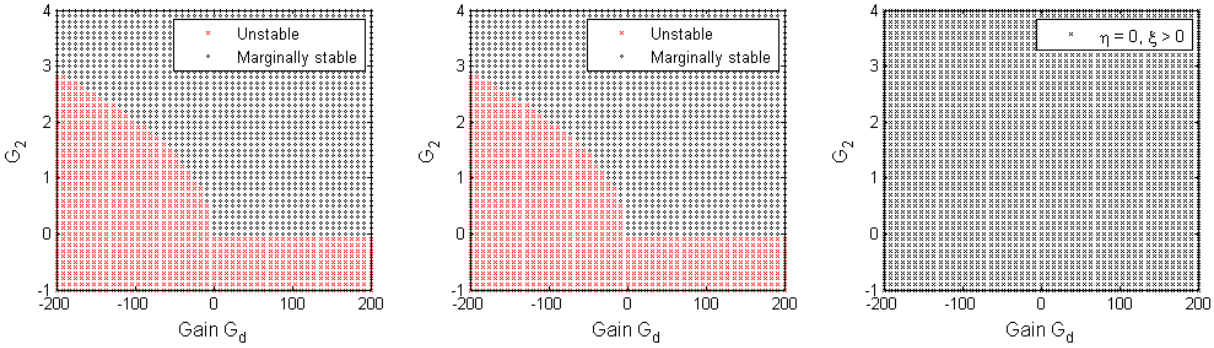

a) $m = 0$ model b) $m > 0$ model c) Positive mass test

Fig. 7. Testcase A1 with controller C_4
Control coil super conductive

- Sets χ_{00n} and χ_{++n} are present. Set χ_{0+} is not present.
- The positive mass test is independent of the gains G_d and G_2. It is satisfied for $R^* > 0$, but in the case of the control coil super conductive, $\eta = 0$, see equation (3xx)
- The vertical axis corresponds to the value of G_2 in C_4, see equation (2).

B. *Testcase C1*

1) *Controller C_1*

This KSTAR model also includes one circuit representing the passive conductors.

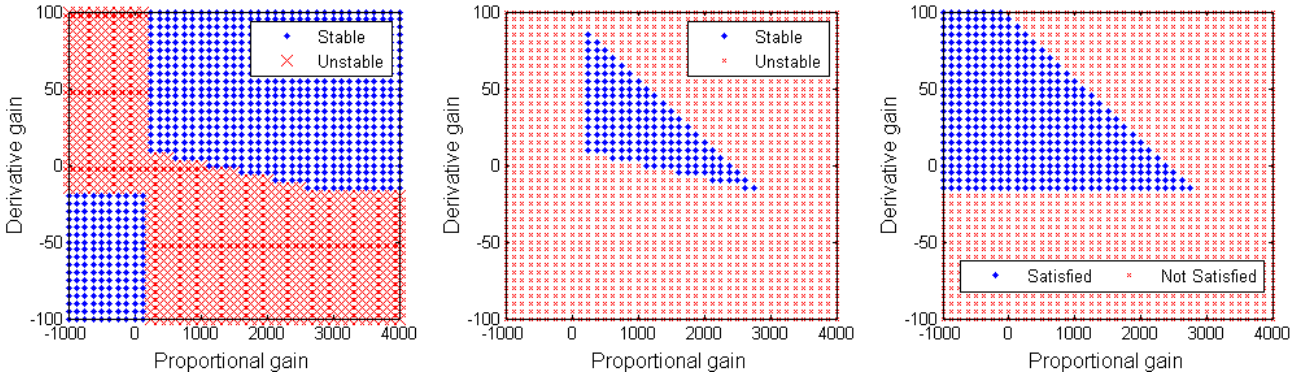

a) $m = 0$ model b) $m > 0$ model c) Positive mass test

Fig. 8. Testcase C1 with controller C_1

- The results are similar to the results from testcase A1. The same sets are present: χ_{++s}, χ_{++n}, χ_{-+n} and χ_{--s}.

Fig. 9 compares the stability areas for the case of a resistive control coil with the case of a super conductive control coil.

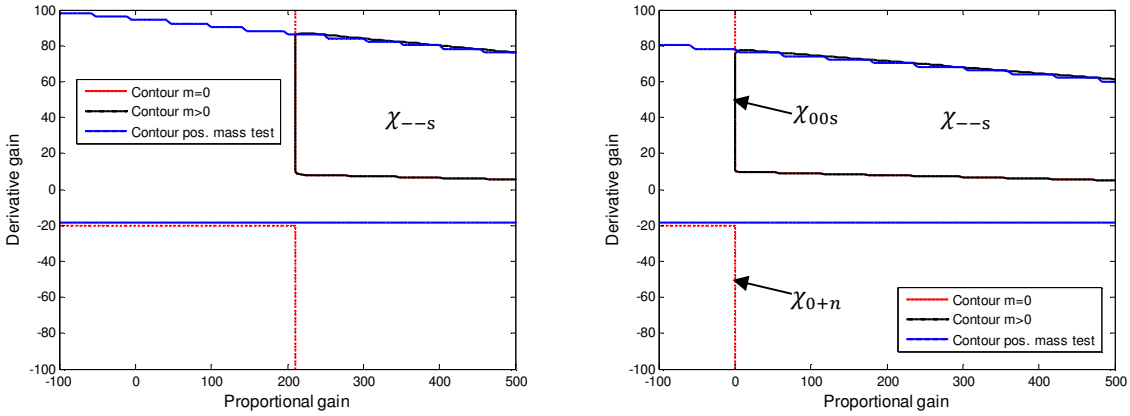

a) $R^*_{pf} = R_{pf}$ b) $R^*_{pf} = 0$

Fig. 9. Influence of the control coil resistance on the sets belonging to testcase C1.

- The set χ_{--s} moves to the left when decreasing the resistance, so less proportional gain is necessary to stabilize the system.
- Decreasing the resistance of the control coil doesn't influence the stability areas as much as it did in testcase A1, due to the presence of the passive conductor of which the is resistance unchanged. Set χ_{--s} stays present, so the $m > 0$ model of this system with one super conductive coil can be stabilized using the PD-controller.

2) *Controller C_2*

- Using only pure derivative gain, the system can be marginally stabilized if and only if the control coil is SC.

3) *Controller C_3*

The proper derivative controller can only marginally stabilize the models, if and only if the control coil is super conductive, see fig. 10.

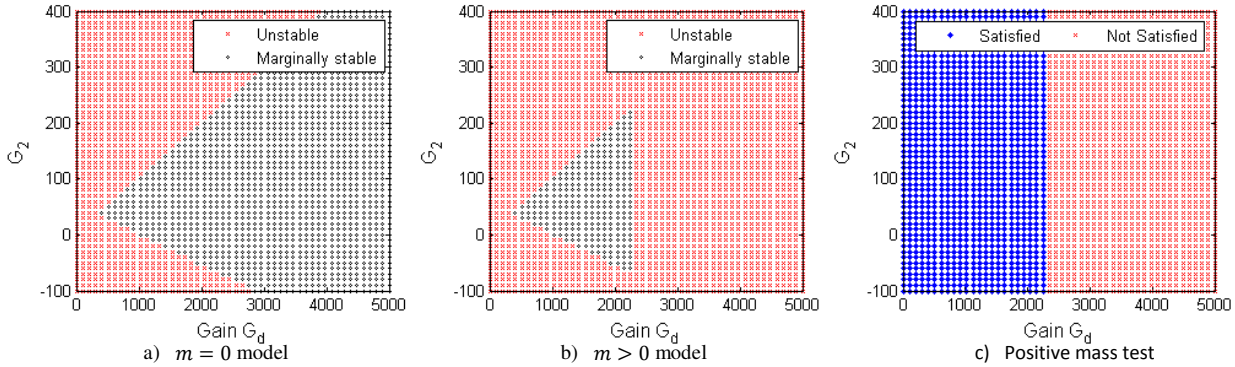

a) $m = 0$ model b) $m > 0$ model c) Positive mass test

Fig. 10. Testcase C1 with controller C_3
Control coil super conductive

- Set χ_{00s}, χ_{++s}, χ_{++n} and χ_{0+n} are present.
- There is an upper limit on the value of G_2. This means the controller C_3 cannot be used as intended, with the pole very far in LHP, i.e. $G_2 \gg 0$ in (2).

4) *Controller C_4*

The strictly proper derivative controller can only marginally stabilize the models, if and only if the control coil is super conductive, see fig. 11.

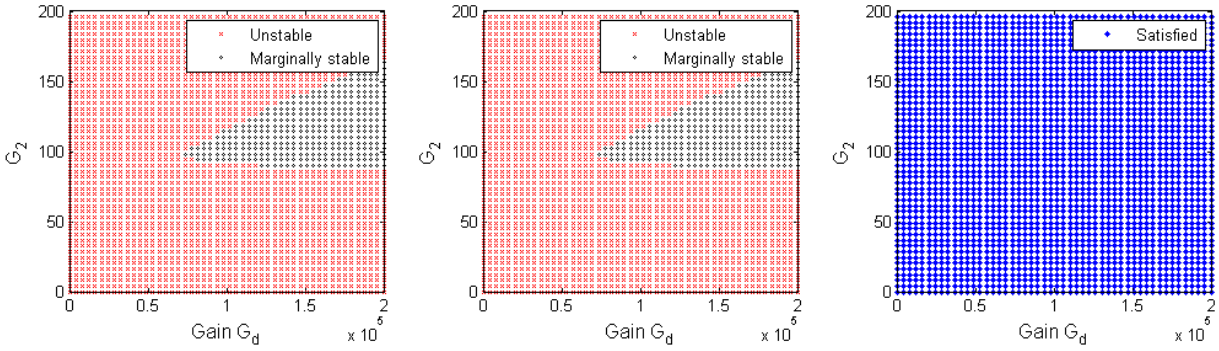

a) $m = 0$ model b) $m > 0$ model c) Positive mass test

Fig. 11. Testcase C1 with controller C_4
Control coil super conductive

- The positive mass test satisfied, and independent of the gains. Set χ_{00s}, and χ_{++s} and present.
- A difference with the results from controller C_3, there the value of G_2 can be increased when the gain G_d is also increased.

C. *Testcase F1*

1) *Controller C_1*

The results for testcase F1 are displayed in fig. 12. Note that the gain values on the axis of this plot are very large, this is to show the boundaries of the sets with stable points.

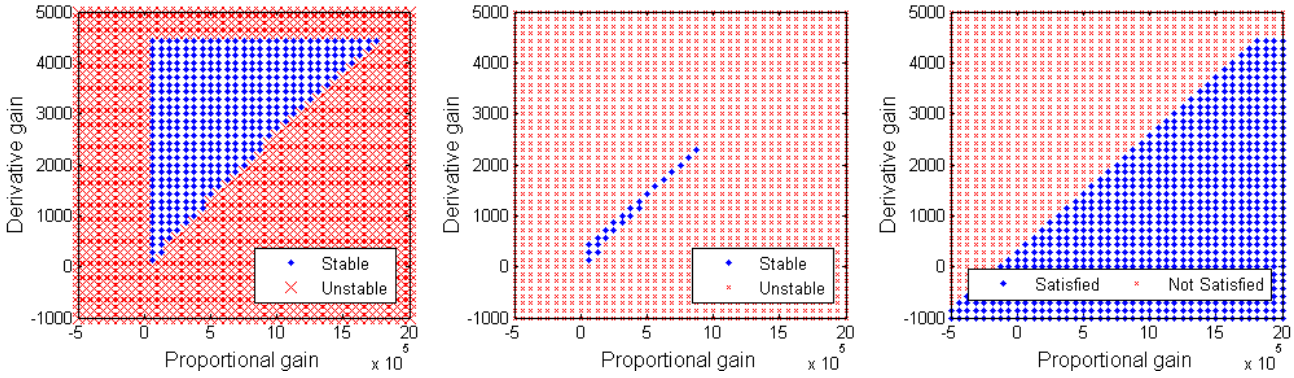

a) $m = 0$ model b) $m > 0$ model c) Positive mass test

Fig. 12. Testcase F1 with controller C_1

- Unlike testcase A1 and C1, there is an upper limit to both the proportional and the derivative gain.
- The derivative gain has an upper limit because too high derivative gain values cause the bandwidth to be higher than the open loop RHP zero (303 rad/s), see fig. 6 in [1].

Fig. 13 shows the results when all control coils are super conductive.

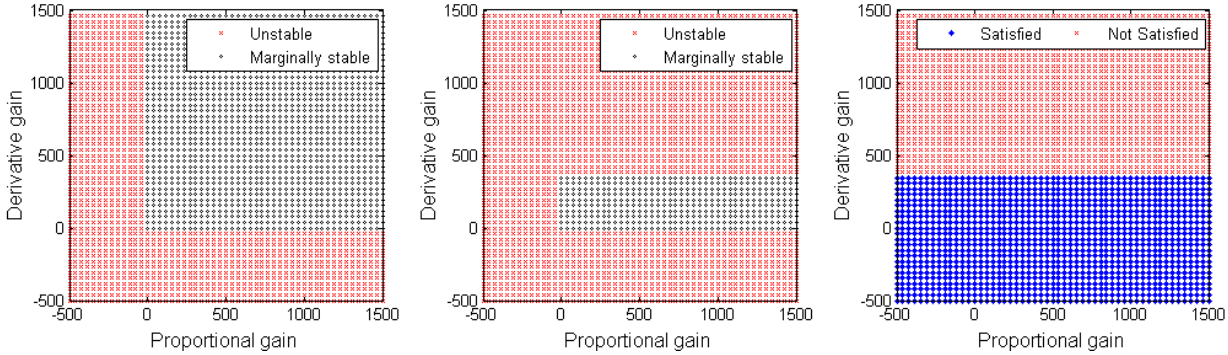

a) $m = 0$ model b) $m > 0$ model c) Positive mass test

Fig. 13. Testcase F1 with controller C_1, with control coils super conductive

- Set χ_{00s}, χ_{++s}, χ_{++n} and χ_{0+n} are present.

2) *Controller C_2*

- All control coils resistive (fig. 12): Pure derivative gain (controller C_2) cannot stabilize the $m = 0$ model. This is another difference with previous testcases.
- All control coils super conductive (fig. 13): The $m = 0$ model can be marginally stabilized by using only derivative gain.

3) Controller C_3

For the case with all control coils resistive, the proper derivative controller cannot stabilize any of the models. Fig. 14 shows the results for all control coils super conductive.

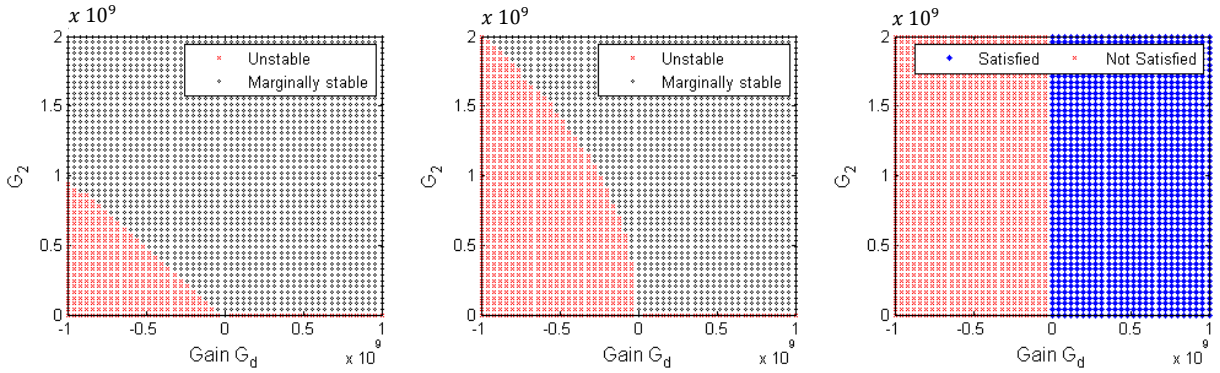

a) $m = 0$ model b) $m > 0$ model c) Positive mass test

Fig. 14. Testcase F1 with controller C_3
All control coils super conductive

- Sets χ_{++s}, χ_{00s}, χ_{++n}, χ_{00n} and χ_{0+n} are present.

4) Controller C_4

For the case with all control coils resistive, the strictly proper derivative controller cannot stabilize any of the models. Fig. 15 shows the results for all control coils super conductive.

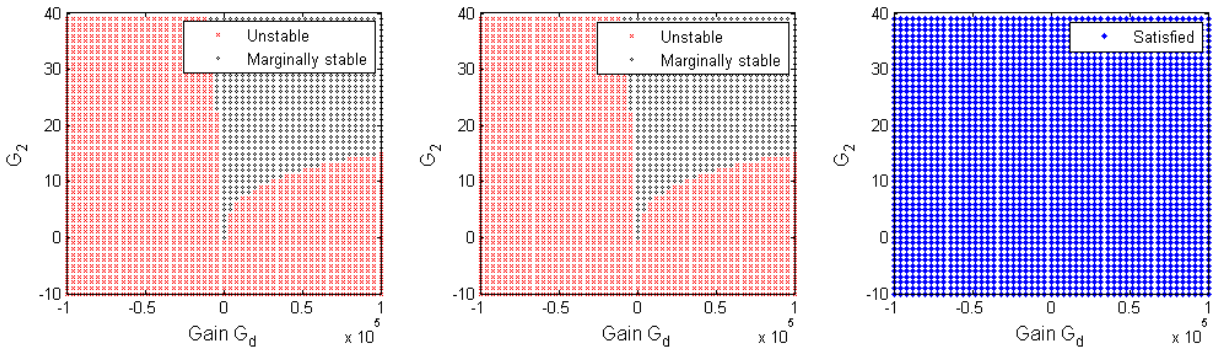

a) $m = 0$ model b) $m > 0$ model c) Positive mass test

Fig. 15. Testcase F1 with controller C_4
All control coils super conductive

- Sets χ_{++s} and χ_{00s} are present.

D. Testcase A2

The results for the single conductor testcase of ITER (fig. 16) are very similar to the results obtained from the single conductor testcase of KSTAR (fig. 3).

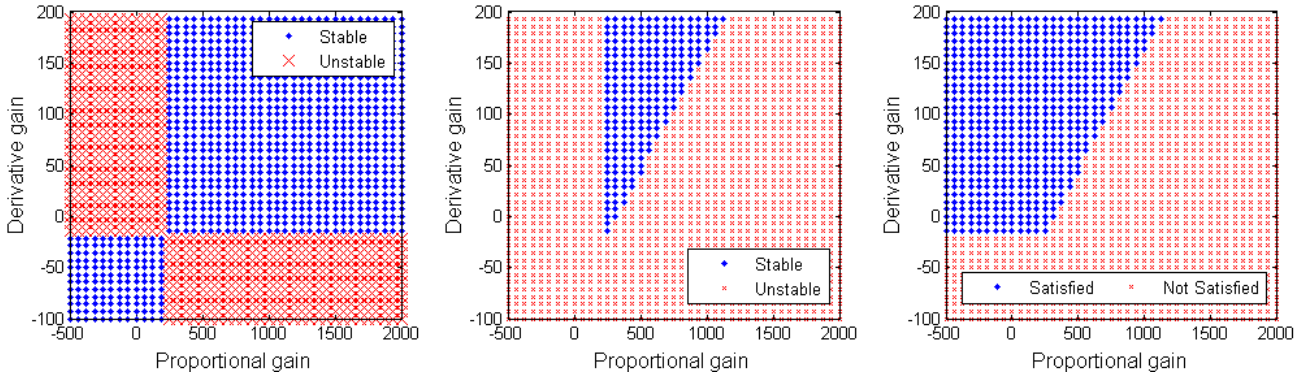

a) $m = 0$ model b) $m > 0$ model c) Positive mass test

Fig. 16. Testcase A2 with controller C_1

E. Testcase C2

The results from testcase C2 with the control coil resistive are displayed in fig. 17.

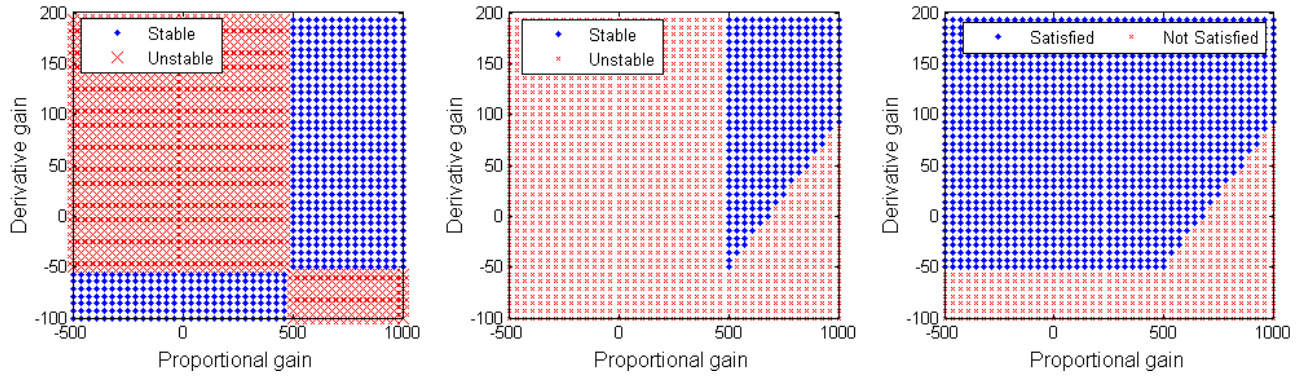

a) $m = 0$ model b) $m > 0$ model c) Positive mass test

Fig. 17. Testcase C2 with controller C_1 with resistive control coils

When the control coils are super conductive, the resulting stability areas have a totally different shape, see fig. 18.

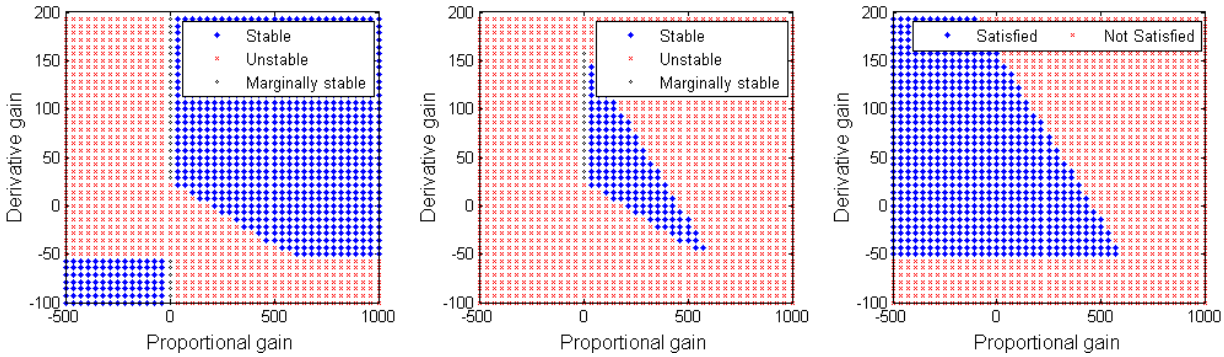

a) $m = 0$ model b) $m > 0$ model c) Positive mass test

Fig. 18. Testcase C2 with controller C_1 with super conductive control coils

Fig. 19 shows how the areas deform when decreasing the control coil resistance.

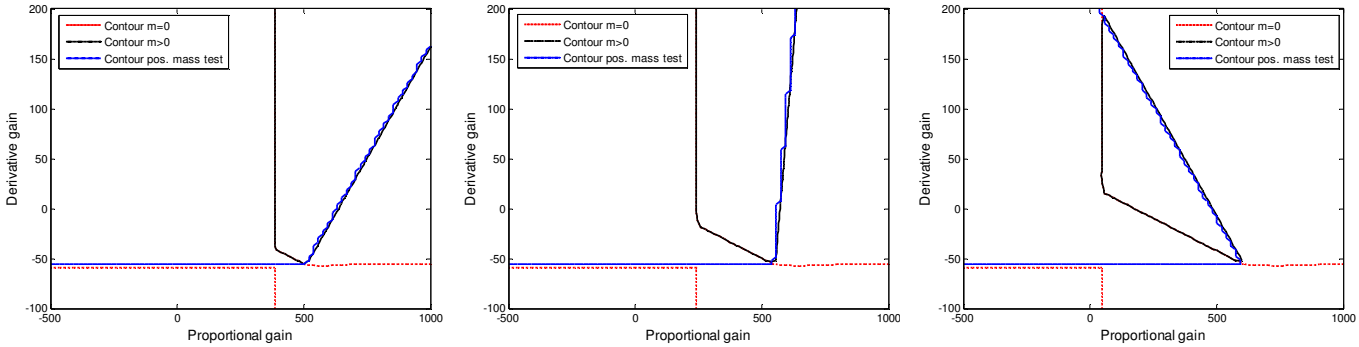

a) $R_{pf}^* = 0.8R_{pf}$ b) $R_{pf}^* = 0.5R_{pf}$ c) $R_{pf}^* = 0.1R_{pf}$

Fig. 19. Testcase C2 with controller C_1 reducing the control coil resistance

- The right boundary of set χ_{---s} rotates while decreasing the control coil resistance. For $R_{pf}^* < 0.4R_{pf}$ this boundary becomes the upper limit of the derivative gain.

F. Testcase F2

The results for testcase F2, with resistive control coils, are displayed in fig. 20.

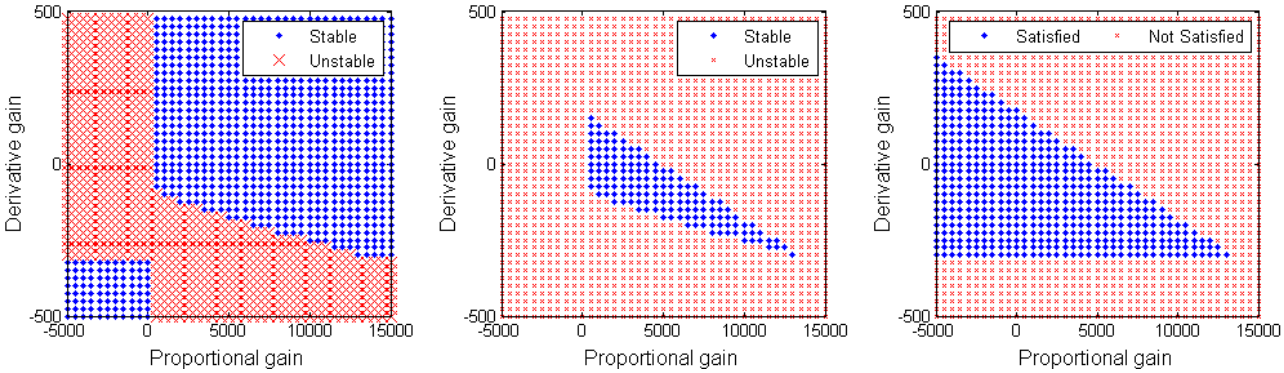

a) $m = 0$ model b) $m > 0$ model c) Positive mass test

Fig. 20. Testcase F2 with controller C_1

Fig. 21 displays the grid for super conductive control coils.

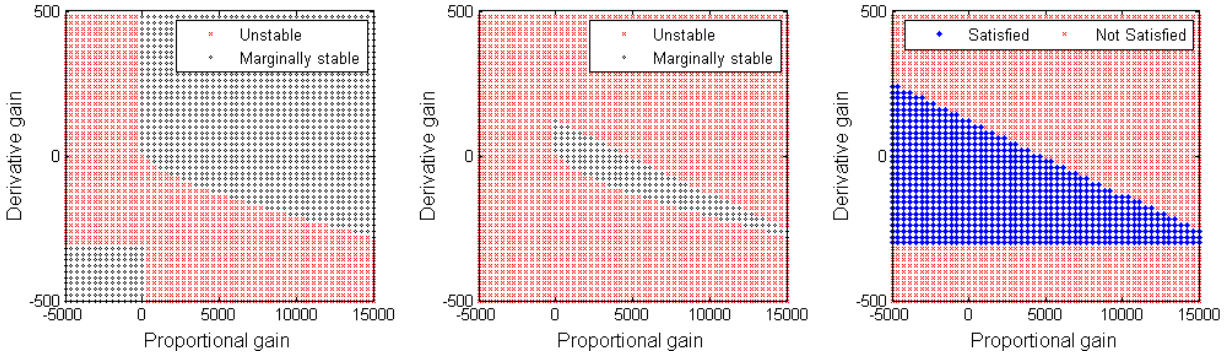

a) $m = 0$ model b) $m > 0$ model c) Positive mass test

Fig. 21. Testcase F2 with controller C_1
With all control coils super conductive

- The $m = 0$ and $m > 0$ model can only be marginally stabilized.

G. Summary testcases

Table 2 provides an overview of all simulation results, both for resistive and for super conductive control coils, and for the four different controllers. Throughout all testcases, a total of eight different sets appear. The ✓–sign marks which sets were found in the simulations by varying the controller gains over a large domain.

Table 2: Summary results from all testcases

	KSTAR								ITER							
	Testcase A1								Testcase A2							
	$0 < R^* \leq R$				$R^* = 0$				$0 < R^* \leq R$				$R^* = 0$			
	C_1	C_2	C_3	C_4	C_1	C_2	C_3	C_4	C_1	C_2	C_3	C_4	C_1	C_2	C_3	C_4
χ_{--s}	✓								✓							
χ_{++s}	✓	✓	✓	✓	✓		✓		✓	✓	✓	✓	✓		✓	
χ_{00s}							✓								✓	
χ_{-+n}	✓	✓			✓				✓	✓			✓			
χ_{++n}	✓		✓		✓		✓	✓	✓		✓		✓			✓
χ_{00n}					✓	✓	✓	✓					✓	✓	✓	✓
χ_{0+n}			✓		✓	✓	✓				✓		✓	✓	✓	
	Testcase C1								Testcase C2							
	$0 < R^* \leq R$				$R^* = 0$				$0 < R^* \leq R$				$R^* = 0$			
	C_1	C_2	C_3	C_4	C_1	C_2	C_3	C_4	C_1	C_2	C_3	C_4	C_1	C_2	C_3	C_4
χ_{--s}	✓				✓				✓				✓			
χ_{++s}	✓	✓	✓	✓	✓	✓	✓	✓	✓	✓	✓	✓	✓	✓	✓	✓
χ_{00s}					✓	✓	✓	✓					✓	✓	✓	✓
χ_{-+n}	✓	✓			✓				✓	✓			✓			
χ_{++n}	✓	✓	✓		✓		✓		✓		✓		✓		✓	
χ_{00n}																
χ_{0+n}			✓		✓	✓	✓				✓		✓	✓	✓	
	Testcase F1								Testcase F2							
	$0 < R^* \leq R$				$R^* = 0$				$0 < R^* \leq R$				$R^* = 0$			
	C_1	C_2	C_3	C_4	C_1	C_2	C_3	C_4	C_1	C_2	C_3	C_4	C_1	C_2	C_3	C_4
χ_{--s}	✓								✓							
χ_{++s}	✓	✓	✓	✓	✓	✓	✓	✓	✓	✓	✓	✓	✓	✓	✓	✓
χ_{00s}					✓	✓	✓	✓					✓	✓	✓	✓
χ_{-+n}	✓								✓	✓						
χ_{++n}	✓	✓	✓		✓		✓		✓	✓	✓		✓		✓	
χ_{00n}							✓									
χ_{0+n}					✓	✓	✓				✓		✓	✓	✓	

For all testcases the growth rate of the tokamak plasma system is calculated and listed in table 3.

Table 3: The growth rate γ for the different testcases

Testcase	$R^* = R$	$R^* = 10^{-4}R$	$R^* = 0$
A1	4.12	$4.12 \cdot 10^{-4}$	0
C1	73.8	55.218	55.216
F1	1.47	$1.8 \cdot 10^{-3}$	$5.4 \cdot 10^{-12}$
A2	11.3	$11.3 \cdot 10^{-4}$	0
C2	8.49	3.336	3.335
F2	3.98	1.286	1.284

Observations:

- Super conductive control coils provide more passive stabilization then resistive control coils.
- The higher order systems are less unstable then the low order systems, because they have more passive stabilizing structures.
- One exception is testcase A1, it is less unstable than C1. This is because the control coil for this testcase was shifted inwards slightly, to provide more stabilization, to get the system out of Ideal Instability (section IV-A in [1]).

III. Observations and conclusions

The controller sets are listed once more in table 4. The colored highlighting provides information about the existence of the different sets.

Table 4: Existence of controller sets

		Positive mass test satisfied			Positive mass test not satisfied		
		$m > 0$ model			$m > 0$ model		
		$\gamma_{cl} < 0$	$\gamma_{cl} = 0$	$\gamma_{cl} > 0$	$\gamma_{cl} < 0$	$\gamma_{cl} = 0$	$\gamma_{cl} > 0$
$m = 0$ model	$\gamma_{cl} < 0$	χ_{--s}	χ_{-0s}	χ_{-+s}	χ_{--n}	χ_{-0n}	χ_{-+n}
	$\gamma_{cl} = 0$	χ_{0-s}	χ_{00s}	χ_{0+s}	χ_{0-n}	χ_{00n}	χ_{0+n}
	$\gamma_{cl} > 0$	χ_{+-s}	χ_{+0s}	χ_{++s}	χ_{+-n}	χ_{+0n}	χ_{++n}

- The light-gray highlighting marks the sets for which was reasoned on beforehand that no controllers will belong to these sets (see Table 1).
- The gray shading marks the sets that appeared in one or more simulations, so from observations it is concluded that these sets are nonempty.
- The sets marked by dark-gray are the remaining sets in the lower triangle of the table. These sets were empty in all testcases. It seems that the $m > 0$ model is always more 'strict' than the $m = 0$ model, i.e. there were never controllers that only stabilized the $m > 0$ model.
  Comparing the form of the characteristic equation of the $m > 0$ model (3a) with the characteristic equation form of the $m = 0$ model (3b) explains this behavior.

$$ma_0\lambda^n + ma_1\lambda^{n-1} + a_2\lambda^{n-2} + \cdots + a_{n-1}\lambda + a_n \quad (3a)$$

$$a_2\lambda^{n-2} + \cdots + a_{n-1}\lambda + a_n \quad (3b)$$

The only difference between these equations is that (3b) does not contain the two highest order terms. These terms

from (3a) are very small compared to the other terms because they contain the small mass m. Therefore the roots following from equation (3b) are almost identical to the roots following from equation (3a). Due to the extra two terms, (3a) has two more poles than (3b). Only this extra pole pair can be responsible for the differences between the two models. So it is known on beforehand that if the $m = 0$ model has an unstable pole, the $m > 0$ model will also contain this unstable pole. So what is happening in sets from the upper triangle of the table is that no poles shared by (3a) and (3b) are in the RHP, only one of the additional poles of (3a) is preventing the $m > 0$ from being asymptotically stable.

The additional pole pair of (3a) provides the same information that results from using the positive mass test. Plotting the sign of the most unstable pole of this additional pole pair, on a grid over different gains, results in exactly the same figures that resulted from evaluating the positive mass test.

Using the above observations, the two question form section *I* can be answered.

1. For what controllers is stability of the physical system correctly predicted when using only the $m = 0$ model? i.e. what controllers are *predictive* or *artifactual?* (See definition 3.2 in [1])
   - The artifactual behavior occurring in the simulations is represented by the sets $\chi_{-+\mathrm{n}}$, $\chi_{0+\mathrm{n}}$ and χ_{0+s}. When the control coils are not super conductive, these sets only appear while using the non proper controllers C_1 and C_2, the (strictly) proper controllers C_3 and C_4 are predictive. Only when the control coils are super conductive, set χ_{0+} appears for controller C_3, never for C_4.
2. Does velocity feedback stabilize the physical system?
   - Controllers C_2, C_3 and C_4 can only marginally stabilize $m > 0$ model when all control coils are super conductive. When the control coils are not super conductive, C_2, C_3 and C_4 cannot stabilize the $m > 0$ model. Controller C_2 could only marginally stabilize the single circuit model, not the two and full circuit models.

REFERENCES

[1] M.J. Beelen, M.L. Walker, G. Witvoet, E. Schuster, M. Steinbuch, *Stability analysis of velocity feedback for the plasma vertical instability in fusion tokamaks*, NYP

[2] D.A. Humphreys, J.R. Ferron, M. Bakhtiari, J.A. Blair, Y. In, G.L. Jackson, H. Jhang, R.D. Johnson, J.S. Kim, R.J. LaHaye, J.A. Leuer, B.G. Penaflor, E. Schuster, M.L.Walker, H. Wang, A.S.Welander and D.G. Whyte, *Development of ITER-relevant plasma control solutions at DIII-D*, Nuclear Fusion, v 47, n 8, Aug. 2007, p 943-51.

[3] J. William Helton, Kevin J. McGown, M.L. Walker, *Conditions for Stabilization of the Tokamak Plasma Vertical Instability Using Only a Massless Plasma Analysis.* Accepted for publication.

[4] M. L. Walker and D. A. Humphreys, *On Feedback Stabilization of the Tokamak Plasma Vertical Instability*, Automatica, vol. 45, no. 3, p.665-674, 2009.